AD-A132 355 HOLOGRAPHIC OPTICAL ELEMENTS WITH ULTRA-HIGH SPATIAL FREQUENCIES(U) AIR FORCE INST OF TECH WRIGHT-PATTERSON AFB OH R C ENGER 1983 AFIT/CI/NR-83-35D 1/2

UNCLASSIFIED F/G 20/6 NL

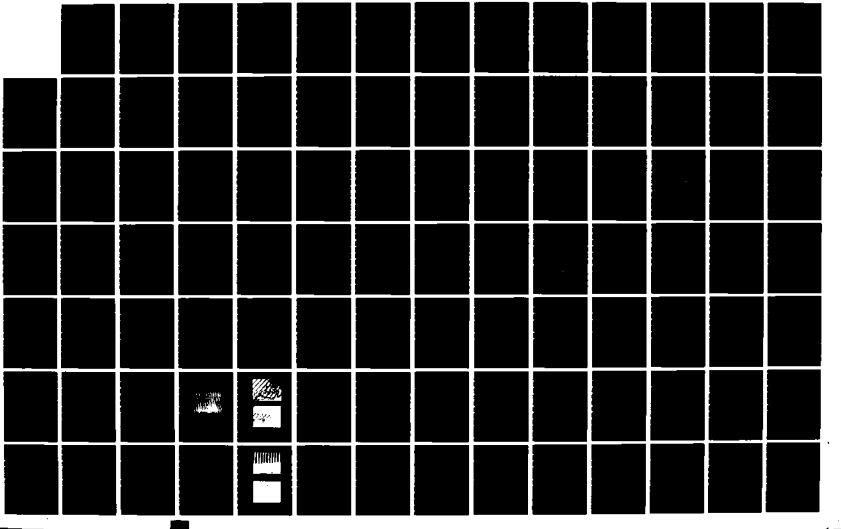

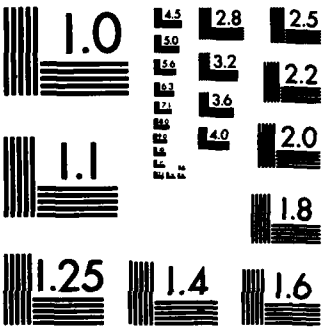

MICROCOPY RESOLUTION TEST CHART
NATIONAL BUREAU OF STANDARDS-1963-A

UNCLASS

SECURITY CLASSIFICATION OF THIS PAGE (When Data Entered)

REPORT DOCUMENTATION PAGE

READ INSTRUCTIONS BEFORE COMPLETING FORM

1. REPORT NUMBER: AFIT/CI/NR 83-35D	2. GOVT ACCESSION NO.: AD-A132355
3. RECIPIENT'S CATALOG NUMBER:	
4. TITLE (and Subtitle): Holographic Optical Elements with Ultra-High Spatial Frequencies	5. TYPE OF REPORT & PERIOD COVERED: THESIS/DISSERTATION
	6. PERFORMING ORG. REPORT NUMBER:
7. AUTHOR(s): Rolf Charles Enger	8. CONTRACT OR GRANT NUMBER(s):
9. PERFORMING ORGANIZATION NAME AND ADDRESS: AFIT STUDENT AT: University of Minnesota	10. PROGRAM ELEMENT, PROJECT, TASK AREA & WORK UNIT NUMBERS:
11. CONTROLLING OFFICE NAME AND ADDRESS: AFIT/NR WPAFB OH 45433	12. REPORT DATE: 1983
	13. NUMBER OF PAGES: 110
14. MONITORING AGENCY NAME & ADDRESS (if different from Controlling Office)	15. SECURITY CLASS. (of this report): UNCLASS
	15a. DECLASSIFICATION DOWNGRADING SCHEDULE:

16. DISTRIBUTION STATEMENT (of this Report)

APPROVED FOR PUBLIC RELEASE; DISTRIBUTION UNLIMITED

17. DISTRIBUTION STATEMENT (of the abstract entered in Block 20, if different from Report)

Approved for [illegible] IAW AFR 190-17

LYNN E. WOLAVER
Dean for Research and Professional Development
Air Force Institute of Technology (AU)
Wright-Patterson AFB OH 45433

18. SUPPLEMENTARY NOTES

APPROVED FOR PUBLIC RELEASE: IAW AFR 190-17

1 SEP 1983

19. KEY WORDS (Continue on reverse side if necessary and identify by block number)

20. ABSTRACT (Continue on reverse side if necessary and identify by block number)

ATTACHED

DTIC ELECTE SEP 1 4 1983 E

DD FORM 1 JAN 73 1473 EDITION OF 1 NOV 65 IS OBSOLETE

UNCLASS

SECURITY CLASSIFICATION OF THIS PAGE (When Data Entered)

83 09 13 102

AD A132355

DTIC FILE COPY

Abstract

This dissertation describes an experimental study of optical elements with ultra-high spatial-frequency surface corrugations in both photoresist and quartz. Details of element fabrication are given and two new applications are suggested.

For the photoresist gratings, angular selectivity, wavelength selectivity, and peak efficiency are investigated. The study shows that optical elements with spatial frequencies in excess of 3000 ℓ/mm and efficiencies greater than 88% can be recorded in subwavelength thick layers of Shipley AZ-1300 series photoresist.

The quartz elements are made via reactive ion etching which faithfully transfers a pattern from a photoresist mask to a fused quartz substrate. The quartz gratings have withstood laser fluxes of 4.17 GW/cm² without sustaining damage and have efficiencies greater than 85%.

Two new applications for substrates with ultra-high spatial-frequency surface corrugations are reported. Such elements at normal incidence are antireflective (AR) with broadband reflection coefficients less than 0.045%. The elements also exhibit artificially produced birefringence making them useful as waveplates. These results may be particularly significant in the UV and IR where damage resistant AR coatings and transparent birefringent materials may not exist.

A brief discussion and accompanying experimental study is included extending holography to the fabrication of integrated circuits with submicron features.

BIBLIOGRAPHY OF KEY WORDS: (For Reference)

Birefringence
Coatings
Diffraction
Holography
Integrated Circuits
Integrated Optics
Laser Damage
Optical Devices
Photolithography
Reflection
Scanners

DTIC COPY INSPECTED

Accession For
NTIS GRA&I
DTIC TAB
Unannounced
Justification
By
Distribution /
Availability Codes
Dist | Avail and/or Special
A

AUTHOR: Rolf Charles Enger

TITLE: Holographic Optical Elements with Ultra-High Spatial Frequencies

MILITARY RANK: Captain

SERVICE BRANCH: United States Air Force

DATE: 1983

NUMBER OF PAGES: 128 (111 pages of text plus 17 introductory pages)

DEGREE AWARDED: Doctor of Philosophy

NAME OF INSTITUTION: University of Minnesota

HOLOGRAPHIC OPTICAL ELEMENTS WITH ULTRA-HIGH SPATIAL FREQUENCIES

A THESIS

SUBMITTED TO THE FACULTY OF THE GRADUATE SCHOOL

OF THE UNIVERSITY OF MINNESOTA

BY

ROLF CHARLES ENGER

IN PARTIAL FULFILLMENT OF THE REQUIREMENTS

FOR THE DEGREE OF

DOCTOR OF PHILOSOPHY

AUGUST 1983

83 09 13 102

DEDICATION

To my wife Lois,

and to my parents,
Carl and Henrietta Enger
and
Kermit and Opal Wolf,

in recognition of their
support and encouragement

Abstract

This dissertation describes an experimental study of optical elements with ultra-high spatial frequency surface corrugations in both photoresist and quartz. Details of element fabrication are given and two new applications are suggested.

For the photoresist gratings, angular selectivity, wavelength selectivity, and peak efficiency are investigated. The study shows that optical elements with spatial frequencies in excess of 3000 ℓ/mm and efficiencies greater than 88% can be recorded in subwavelength thick layers of Shipley AZ-1300 series photoresist.

The quartz elements are made via reactive ion etching which faithfully transfers a pattern from a photoresist mask to a fused quartz substrate. The quartz gratings have withstood laser fluxes of 4.17 GW/cm^2 without sustaining damage and have efficiencies greater than 85%.

Two new applications for substrates with ultra-high spatial frequency surface corrugations are reported. Such elements at normal incidence are antireflective (AR) with broadband reflection coefficients less than 0.045%. The elements also exhibit artificially produced birefringence making them useful as waveplates. These results may be particularly significant in the UV and IR where damage resistant AR coatings and transparent birefringent materials may not exist.

A brief discussion and accompanying experimental study is included extending holography to the fabrication of integrated circuits with submicron features.

Acknowledgements

Throughout this study I have been blessed with the help of many kind people. A list of all their names would be prohibitively long. However, I would like to express my sincere gratitude to Professor Steven Case for his guidance, direction, enthusiasm, and constructive criticism concerning this research. I am also deeply indebted to Stephen Gilbert of the University Microelectronics Laboratory for his extensive help regarding photoresist processing and reactive ion etching. I would also like to thank my colleagues Larry Konicek, Paul Haugen, Ron Indeck, Chris Henze, Jeff Jalkio, Dan Hulsey, and Hartmut Bartelt for their helpful suggestions and assistance, and my program manager, Lt Col John Kitch, Jr., for his guidance and support.

During the course of this research, several companies offered their facilities and personnel to assist in this research. They include: Control Data Corporation, Honeywell Corporation, VERTIMAG, 3M, the United States Air Force Academy and Anelva. I am especially appreciative of Tom Roberts, Linda Tennis, and the Control Data Corporation who together took most of the Scanning Electron Microscope pictures and to the Honeywell Corporation where the reactive ion etching was done. I also wish to thank Lt Col Barry Crane and Robert O'Connel for performing the laser radiation testing, and to John Schultz and Don Kerfeld for their work on grating replication.

This research was supported by the Army Research Office and the Air Force Office of Scientific Research under contract #DAAG 29-81-K-0033. Other monetary remuneration was provided by the Air Force Institute of Technology. I am very grateful for this support.

Finally, I would like to extend a special word of thanks to my wife and daughters Tiffany and Holly who lovingly supported me throughout the long months of study and research.

"I can do all things through Christ who strengthens me"

Philippians 4:13

"And we know that all things work together for good to those who love God, to those who are called according to His purpose."

Romans 8:28

Contents

Contents

List of Figures

List of Tables

List of Symbols

A	magnitude of plane wave
B	magnitude of plane wave
B'	factor depending on exposure time and slope of film's amplitude transmittance vs. exposure curve.
d	grating period
D	grating thickness
e	2.7182818 (also "exp")
$\hat{E}_1$	plane wave
$\hat{E}_2$	plane wave
$\hat{E}_{IN}$	incident electric field vector
$\hat{E}_{out}$	electric field vector emerging from linear analyzer
E_x	magnitude of incident electric field vector
E_t	electric field vector emerging from grating
f	spatial frequency
F_e	fraction of exposed photoresist molecules
f_ℓ	focal length of lens
F_u	fraction of unexposed photoresist molecules
h	Planck's constant
I	intensity
I_{IN}	intensity of beam used to illuminate a grating or photoresist
I_{max}	maximum intensity of interference fringe
I_{min}	minimum intensity of interference fringe
I_{out}	intensity (also I_A and I_B)
I_{R1}	intensity of reflection off prism
I_{R2}	intensity of reflection off grating

$I(y)$	irradiance at position y in photoresist where y measures photoresist depth
I_o	intensity of zeroth order
I_1	intensity of first diffracted order
j	$\sqrt{-1}$
k	wave number
Δm	amount of photoresist material removed by developer
N	diffractive order number
n	index of refraction
n_x	index of refraction -- x direction
n_y	index of refraction -- y direction
N_o	initial photoresist molecular density
N_1	density of unexposed photoresist molecules
Q	grating Q factor
R	ratio defined in Eq. 30
$\hat{r}$	unit directional vector
r_f	diffraction limited radius of the focal spot of lens
r_1	rate developer attacks exposed photoresist molecules
r_2	rate developer attacks unexposed photoresist molecules
T	development time
t	time
t_f	amplitude transmittance of film
T_p	transmittance of a polarizer
V	fringe visibility
w	diameter of lens
x	spatial variable

y	spatial variable
α	absorption cross section of photoresist molecule
η	grating efficiency (η_{max} is maximum efficiency)
η_q	quantum efficiency
$\phi(r)$	phase angle (also ϕ)
$\Delta\phi_n$	change in phase due to a grating
λ_o	free space wavelength
π	3.1415926
$\psi(r)$	phase angle
θ	for a photoresist grating, the angle inside the glass substrate between the incident light and the glass-resist normal
θ_B	Bragg angle
θ_{IN}	illumination angle measured outside a grating substrate
θ_N	emergence angle of the Nth diffracted order
θ_p	angle between polarizer major axis and x axis
θ_1	incident angle of one beam during holographic exposure
θ_2	incident angle of one beam during holographic exposure
ν	light frequency
ω	angular speed

List of Abbreviations

AM	the part of the day from midnight until noon
AMD	angle of minimum deviation
AR	antireflective or antireflection
Au	gold
AZ	Shipley designation for their photoresist and photoresist developer
BS	beam splitter
CA	critical angle
DCR	model of Quanta Ray Laser
DI	deionized
F	film plane
FWHM	full width at half max
GaAs	gallium arsenide
HOE	holographic optical element
IC	integrated circuit
IR	infrared
L	lens
M	mirror
Nd	neodymium
SEM	scanning electron microscope
SiO_2	silicon dioxide
SF	lens pinhole spatial filter
TBA	theoretical Bragg angle
UV	ultraviolet
YAG	yttrium aluminum garnet
3M	Minnesota Mining and Manufacturing Company

List of Units

cm	centimeter
GHz	gigahertz
GW	gigawatt
Hz	hertz
J	joule
ℓ	line
min	minute
mJ	millijoule
mm	millimeter
nm	nanometer
nsec	nanosecond
rpm	revolutions per minute
°	degree
μm	micrometer

I. Introduction

Holographic optical elements (HOEs) with high diffraction efficiency can often be used as replacements for conventional optical elements. For example, supermarket scanners which optically read the price code preprinted on merchandise now use rotating discs comprised of a series of HOEs, each diffracting light through a slightly different angle. The result is a lightweight device which efficiently distributes laser light through a very complex pattern[1,2].

When faced with the problems of production technology, such as in the marketing of scanners, the ability to cheaply reproduce HOEs from a master has led researchers to study phase holograms recorded in photoresist. Photoresist HOEs have surface relief features which make them attractive candidates for potentially inexpensive replication using various embossing or deposition techniques.

Unfortunately, the ease with which transmission photoresist HOEs can be replicated has traditionally been offset by limited diffraction efficiency (<40%). Without high efficiency, the use of HOEs is often impractical. However, recent theoretical[3] and experimental[2] studies indicate that deep groove diffractive elements formed in relatively thin media can exhibit diffraction efficiencies well in excess of 40%.

The motivation for our study, which predates references 2 and 3, was the desire to demonstrate that surface relief

holograms can have high efficiencies in a single diffracted order. Thus, we limited our study to consideration of HOEs with spatial frequencies so large that all but one diffracted order is evanescent. To date, we have produced HOEs with first-order diffraction efficiencies greater than 88%.

Background

The idea of diffraction-based optics dates back to 1871 when Lord Rayleigh constructed a Fresnel Zone Plate. However, it was not until Gabor proposed his principle of wavefront reconstruction and Leith and Upatnieks introduced off-axis holographic techniques that HOE development rapidly advanced[4].

As early as 1968, researchers were successful in using photoresist to make reflection holographic diffraction gratings. In that year, Sheridon[5] fabricated blazed reflection gratings with 73% diffraction efficiency and predicted that 90% efficiency should be possible. Sheridon's results were later confirmed by Rudolph and Schmahl[6] and improvements have been made since. However, for some optical applications, such as laser beam scanning, transmissive diffractive elements are preferred, thus prompting our study of such elements.

Early work with photoresist transmission gratings was directed towards insuring linearity for use in image forming holograms, although optimizing efficiency was recognized as

important. In 1970 Bartolini et al.[7] reported average efficiencies of about 3%. Concurrently, Beesley and Castledine[8] reported photoresist gratings with transmission efficiencies "much lower" than 30%. In 1974, Bartolini[9], again striving for linearity, reported transmission efficiencies of 5%. Later work by Iwata and Tsujiuchi[10] proved that 25% efficiencies were possible while Kurtz and Owen[11], in a subsequent review paper, implied that 30% transmission holograms had been produced.

Work in the mid 70's was limited mainly to the use of photoresist as a mask for etching or milling as researchers turned to dichromated gelatin for high efficiency applications. Only recently has high efficiency been achieved with photoresist; the result of our work[12], and the simultaneous efforts of Kramer[2].

Approach

In this thesis we investigate the properties of diffractive optics recorded holographically in photoresist and describe the fabrication techniques employed to achieve efficiencies greater than 88%. Unfortunately, our findings include the fact that photoresist HOEs are easily damaged. However, we have found a way to minimize this problem by using reactive ion etching to transfer the holographic recording into a quartz substrate. Our experiments demonstrate that such transfer faithfully reproduces the surface

relief features and diffractive properties of the photoresist masks including diffraction efficiencies greater than 85%.

We also report on two new applications for HOEs with high spatial frequencies. First, we have discovered that our deep-groove diffraction gratings are very damage resistant and have antireflective (AR) properties rivaling the best AR coatings. Secondly, we report on tests which show that these gratings exhibit artificially produced birefringence making them useful as waveplates. These results may be particularly significant in the UV and IR where damage resistant AR coatings and transparent birefringent materials may not exist.

II. Photoresist as a Recording Medium

The photographic properties of photoresists have been described extensively[9,11,13-15]. Photoresist is a light sensitive organic material which can be easily applied to a flat substrate, usually by flooding the substrate with resist and then spinning at speeds between 3000 and 6000 rpm. Thus, it can be conveniently applied to good quality optical substrates, allowing the production of high quality optics with few defects and low scattering levels.

Because photoresist involves a molecular process, it has no granularity. Thus, spatial frequencies in excess of 5000 line pairs/mm can be recorded in it[15].

Types of Photoresist

There are two types of photoresist: negative and positive. When negative photoresist absorbs light, the organic molecules form cross linkages which harden the resist. When developed, the developer washes away the unexposed molecules, leaving the exposed molecules essentially untouched. Unfortunately, because substrate adhesion depends upon the number of cross linkages formed, negative photoresists are difficult to work with when recording holographic optical elements with submicron features. Frequently, the exposures needed to achieve good adhesion exceed those needed to optimize the holographic process. Thus, the fine lines recorded

in holographic optics tend to separate from the substrate due to insufficient exposure[16,17].

During our research we used positive photoresist in which light destroys the cross linkages. Development then washes away the exposed molecules; i.e. the molecules with destroyed cross linkages.

There are several resist manufacturers including Shipley, Kodak, and MacDermid. A chart comparing the properties and performance characteristics of various photoresists can be found in reference 16. We chose Shipley AZ-1300 series photoresists, manufactured by the Shipley Co., Inc., Newton, Massachusetts, because of their proven high resolution. Shipley AZ-1350 is the most widely used photoresist for holographic applications[16].

Shipley AZ-1350 Characteristics

Shipley AZ-1350 photoresist has a sensitivity of about 1/25,000 that of Kodak 649F film and is most sensitive to light between 340 nm and 450 nm[11]. The specific characteristics of Shipley AZ-1350B and AZ-1350J photoresist, the two types we worked with, are listed in Table I as compiled from Shipley technical data[18] and personal communications with company representatives[19]. Recently, Shipley introduced an AZ-1400 series of photoresists, similar to the AZ-1300 series, designed for microelectronics applications requiring high resolution and superior edge acuity[18]. AZ-1400 series

Table I
Characteristics of Shipley Photoresist

	AZ-1350B	AZ-1350J
Solid Content, approx.	17%	31%
Type of Solution	solvent base	solvent base
Specific Gravity (25° C)	1.000 ± 0.010	1.040 ± 0.010
Flash Point	44° C	44° C
Index of Refraction (Soft baked; at 632.8 nm)	1.64 ± 0.01	1.64 ± 0.01
Coating Thickness, range	0.3 - 0.5 μm	1.5 - 2.2 μm

(From Refs 18 and 19)

photoresist has a leveling agent to prevent striations from forming in the resist[19].

Shipley publishes charts showing the thickness achieved when spinning their photoresists at various spin speeds. AZ-1350B is the thinnest resist and can be spun to thicknesses between 0.3 μm and 0.5 μm. AZ-1370 is the next thickest, capable of producing film thicknesses between 0.9 μm and 1.3 μm[18]. Note that there is a range of thicknesses, from 0.5 μm to 0.9 μm that cannot be achieved by either resist. During our research we found it necessary to obtain film thicknesses within this range. Thus, we spun a mixture of AZ-1350B and AZ-1350J. Table II lists AZ-1350B/AZ-1350J mixture ratio and spin rates required to achieve various intermediate film thicknesses. All

Table II
Intermediate Photoresist Film Thicknesses

Film Thickness (μm)	AZ-1350B/AZ-1350J Ratio	30 second Spin Rate (rpm)
0.55 ± 0.02	22/11	6000
0.62 ± 0.01	22/11	5500
0.71 ± 0.01	14/11	5500
0.75 ± 0.01	14/11	4500

measurements were made with a Taly Alpha Step after baking the resist for 40 minutes at 80° C and then developing it for 30 seconds in AZ developer diluted 1:1 with deionized (DI) water.

One of the significant contributions of this research is the extension of the resolution limits of AZ-1350 photoresist. As a result of experimental study, Bartolini concluded in a 1977 publication that the maximum useful recording spatial frequency of Shipley AZ-1350 photoresist is 1500 ℓ/mm. He reported that holographic diffraction efficiency drops off markedly once a spatial frequency of 1500 ℓ/mm is exceeded, dropping from a normalized value of 1.0 at 1500 ℓ/mm to a value of approximately 0.5 at 2000 ℓ/mm[16]. However, as we demonstrate in subsequent chapters of this thesis, we have obtained diffraction efficiencies exceeding 88% in Shipley AZ-1350 photoresist for spatial frequencies of 3000 ℓ/mm.

Theoretical Review of Photoresist Processing

In this section we briefly describe a theoretical model which mathematically describes the interactions between light, photoresist, and photoresist developer[16].

When light is incident on positive photoresist, the energy absorbed as a function of depth, y, is given by

$$I(y) = I_{IN} e^{-\alpha N_1 y} \tag{1}$$

where I_{IN} is the irradiance incident at the photoresist surface, N_1 is the density of the unexposed photoresist molecules available to absorb the incident radiation, and α is the absorption cross section of the photoresist molecule.

Assuming the photoresist layer is thin (a few microns) and the percentage of light absorbed is small, then $I(y) \cong I_{IN}$ and the rate at which previously unexposed molecules become exposed molecules is given by

$$\frac{-dN_1(t)}{dt} = \eta_q \left[\frac{I_{IN}}{h\nu}\right] \alpha N_1(t) \tag{2}$$

or

$$N_1(t) = N_o \exp\left[\frac{-\eta_q \alpha}{h\nu} (I_{IN} t)\right] \tag{3}$$

where N_o is the initial photoresist molecular density, $I_{IN}/h\nu$ is the number of photons available for absorption and η_q is the quantum efficiency; i.e. the number of molecules which after absorbing a photon will be washed away during development. The quantum efficiency accounts for the fact

that some molecules will not wash away during development even though they have absorbed a photon. Such molecules are still considered unexposed.

In Eq. 3, $\eta_q \alpha / h\nu$ is known as the exposure constant for positive photoresist (cm^2/mJ) and $I_{IN}t$ is the photoresist exposure (mJ/cm^2).

Using the above formalism, photoresist etch depth can be calculated as a function of exposure. Define F_u as the fraction of unexposed photoresist molecules. Thus,

$$F_u = \frac{N_1(t)}{N_o} = \exp\left[\frac{-\eta_q \alpha}{h\nu}(I_{IN}t)\right] \tag{4}$$

and the fraction of exposed photoresist molecules is given by

$$F_e = 1 - F_u \tag{5}$$

The photoresist model assumes that in positive photoresist development, the exposed and unexposed molecules are attacked by the developer at different rates, r_1 and r_2, respectively. Thus, the amount of material, Δm, removed at any point y by the developer will be

$$\Delta m = T(F_e r_1 + F_u r_2) \tag{6}$$

where T is the development time. Using Eq. 4, Eq. 6 can be expressed in terms of photoresist exposure, $I_{IN}t$, to obtain

$$\Delta m = T\left\{r_1 - (r_1 - r_2)\exp\left[\frac{-\eta_q \alpha}{h\nu}(I_{IN}t)\right]\right\} \tag{7}$$

Thus, if no exposure occurs, ($I_{IN}t = 0$) then photoresist

removal, as expected, depends only on the rate developer attacks unexposed molecules. However, if the exposure is very large, then $\Delta m \cong r_1 T$ and developer attack depends solely on the exposed etch rate. This second case is usually the goal when making holographic optical elements, especially high efficiency diffraction gratings. If exposed areas etch solely at the faster exposed rate, there is little chance for unexposed areas to etch at all. The result is large aspect ratios; which was the goal of our research.

Experimental Considerations

In addition to the theoretical considerations, we offer, *in this section, a few* general suggestions regarding the handling of photoresist, and in particular Shipley AZ-1350B. Specific processing techniques will be discussed in the next chapter.

Because photoresist is light sensitive, it should not be exposed to white light. However, since photoresist is very insensitive to long wavelength visible light, we found AZ-1350 photoresist could be safely processed under gold fluorescent light for extended periods (in excess of 1 hour).

Imperfections in substrate surfaces, including stray dust particles laying on the surface, cause streaking of the photoresist during spin application. Thus, scratched or

chipped substrates should not be used and substrates should be blown clean with dry gas immediately before coating.

Another cause of inconsistent or nonuniform coating is insufficient photoresist applied to the substrate prior to spinning. Thus, substrates should be flooded with excess photoresist before spinning. The excess photoresist is automatically thrown off due to centripetal acceleration.

Photoresist dries rapidly when exposed to air. Solvent in bottles left uncovered can evaporate, resulting in a thickening of the photoresist. This thicker photoresist, when spun, produces a thicker film coating. Thus, to ensure consistent results, photoresist bottles must be quickly capped after each use.

The quick drying property of photoresist can also present problems when applying the resist from a device such as a syringe. When coating several substrates in succession, small amounts of the photoresist can begin to dry in the tip of the syringe during the time required to process a given sample (i.e. spinning of the resist-flooded substrate plus the alignment and precleaning with dry gas of the next substrate). This semi-dried photoresist can dislodge when the next substrate is flooded, producing visible worm-like streaks in the photoresist coating. To avoid this problem, a small portion of resist should be discharged from the syringe prior to the flooding of each substrate. In most cases, this discharge will contain any partially dried

resist and will prevent contamination of the substrate surface.

When spin coating substrates, resist may occasionally flow underneath the substrate. This is especially true when vacuum chucks are used to hold the substrate during coating. Contamination of the back of the substrate can be minimized by applying all photoresist to the center of the substrate during flooding. The resist will naturally flow outward from the substrate center. Backside contamination is usually avoided if spinning is begun before the resist reaches the substrate edges.

If some photoresist does reach the back of the substrate, it can be removed with acetone. Care must be taken to avoid getting acetone on the front surface as acetone will dissolve photoresist, resulting in an uneven coating.

III. Holographic Grating Construction in Photoresist

For years, diffraction gratings have been made by mechanically ruling (scribing) a substrate with a sharp stylus. Although very good gratings are produced using this technique, stylus size limits grating spatial frequency; small errors in drive motors lead to periodic ruling errors; occasional deviations in machine performance introduce random errors[20]; and, most importantly, there is essentially no way to introduce focal power, multiplexed elements, or aspherics. However, holography proves capable of solving most of these problems.

Holography

Wavefront reconstruction, now known as holography, was invented by Dennis Gabor in 1948[21]. At that time, the technique was applied to electron microscopy. However, it was not until Leith and Upatnieks coupled holography with the new technology of lasers, that holography came of age.

Lasers are ideally suited to holography because of their inherent coherence. If one properly brings two coherent light beams together, a stable interference pattern is obtained. Bright regions occur where the beams interfere constructively while dark regions correspond to points of destructive interference. It is because of the coherence of these two beams that the pattern of bright and dark regions does not change with time.

If a photographic emulsion is placed in the region of interference, the interference pattern can be recorded. This is true no matter how complicated the interference pattern, up to the resolution limit of the emulsion itself. Thus, even the complex interference pattern produced by an aspheric lens or a combination of lenses can be faithfully recorded. When a photographic record is made of this interference pattern, sufficient information is recorded about the phase and amplitude of the interfering light so that reconstruction of this interference pattern is possible by reilluminating the hologram with coherent light.

For example, consider two coherent plane waves incident on a photographic emulsion with amplitudes

$$\vec{E}_1 = A e^{-j\phi(r)} \hat{r} \tag{8}$$

and

$$\vec{E}_2 = B e^{-j\psi(r)} \hat{r} \tag{9}$$

Because these two waves interfere coherently, the resulting intensity is

$$I = (\vec{E}_1 + \vec{E}_2)\cdot(\vec{E}_1 + \vec{E}_2)^* \tag{10}$$

$$= A^2 + B^2 + 2AB\cos[\psi(r) - \phi(r)] \tag{11}$$

Thus, even though the photographic emulsion records only the intensity, the intensity itself contains information about the phase difference $[\psi(r) - \phi(r)]$. However, note that $\vec{E}_1$

and $\vec{E}_2$ must be coherent. If not, the phase difference $[\psi(r) - \phi(r)]$ will not be constant in time and thus will not be uniquely recorded.

When the intensity distribution of Eq. 11 is recorded by a photographic emulsion, a new factor, B', is introduced which depends on the exposure time and on the slope of the film's amplitude transmittance vs. exposure curve. Thus, the amplitude transmittance of the film becomes

$$t_f = B'(|\vec{E}_1|^2 + |\vec{E}_2|^2 + \vec{E}_1^* \cdot \vec{E}_2 + \vec{E}_1 \cdot \vec{E}_2^*) \tag{12}$$

(assuming linear recording).

Reconstruction of the original plane wave, $\vec{E}_1$, occurs when the film is reilluminated with a coherent reconstruction wave that is an exact duplication of the original wave, $\vec{E}_2$. The result of this reillumination is

$$\vec{E}_2 t_f = B'(\vec{E}_1 \cdot \vec{E}_1^* \vec{E}_2 + \vec{E}_2 \cdot \vec{E}_2^* \vec{E}_2 + \vec{E}_1^* \cdot \vec{E}_2 \vec{E}_2 + \vec{E}_1 \cdot \vec{E}_2^* \vec{E}_2) \tag{13}$$

Rewriting the fourth term, using Eqs. 8 and 9, we have

$$B' \vec{E}_1 \cdot \vec{E}_2^* \vec{E}_2 = AB'B^2 e^{-j\phi(r)} \hat{r} \tag{14}$$

which, except for a multiplicative constant is the original plane wave, $\vec{E}_1$[22].

Successful holography depends upon several factors. First, the interference fringes should be of high contrast, quantitatively measured by the fringe visibility

$$V = \frac{I_{max} - I_{min}}{I_{max} + I_{min}} \tag{15}$$

where I_{max} and I_{min} are the maximum and minimum intensities of the interference fringes in the observation plane[23]. High fringe visibility maximizes the chance that exposed areas of photoresist will etch away at the exposed rate, $r_1 T$, and minimizes the etch rate in the unexposed areas (i.e. makes $I_{IN}t$ as close to zero as possible--see Chapter II). This maximizes the aspect ratio of the grating fringes and leads to high efficiency[3].

Secondly, successful holography requires fringe stability during film exposure. Fringe stability minimizes exposure in areas of otherwise destructive interference and thus minimizes the development rate in these areas. As before, this minimization is required if maximum aspect ratios and thus maximum diffraction efficiencies are to be obtained.

Grating Recording Geometry

In the simplest case, two coherent plane waves, when brought together, will interfere to produce a series of parallel bright and dark bands; i.e. a grating-like pattern. If incident on film at angles θ_1 and θ_2 as in Fig. 1 (where θ_2 is negative) they will record a pattern with spatial frequency

$$f = \frac{1}{d} = \frac{1}{\lambda_o}(\sin\theta_1 - \sin\theta_2) \qquad (16)$$

where d is the grating period and λ_o is the free space wavelength. In the limit, the minimum grating period recordable

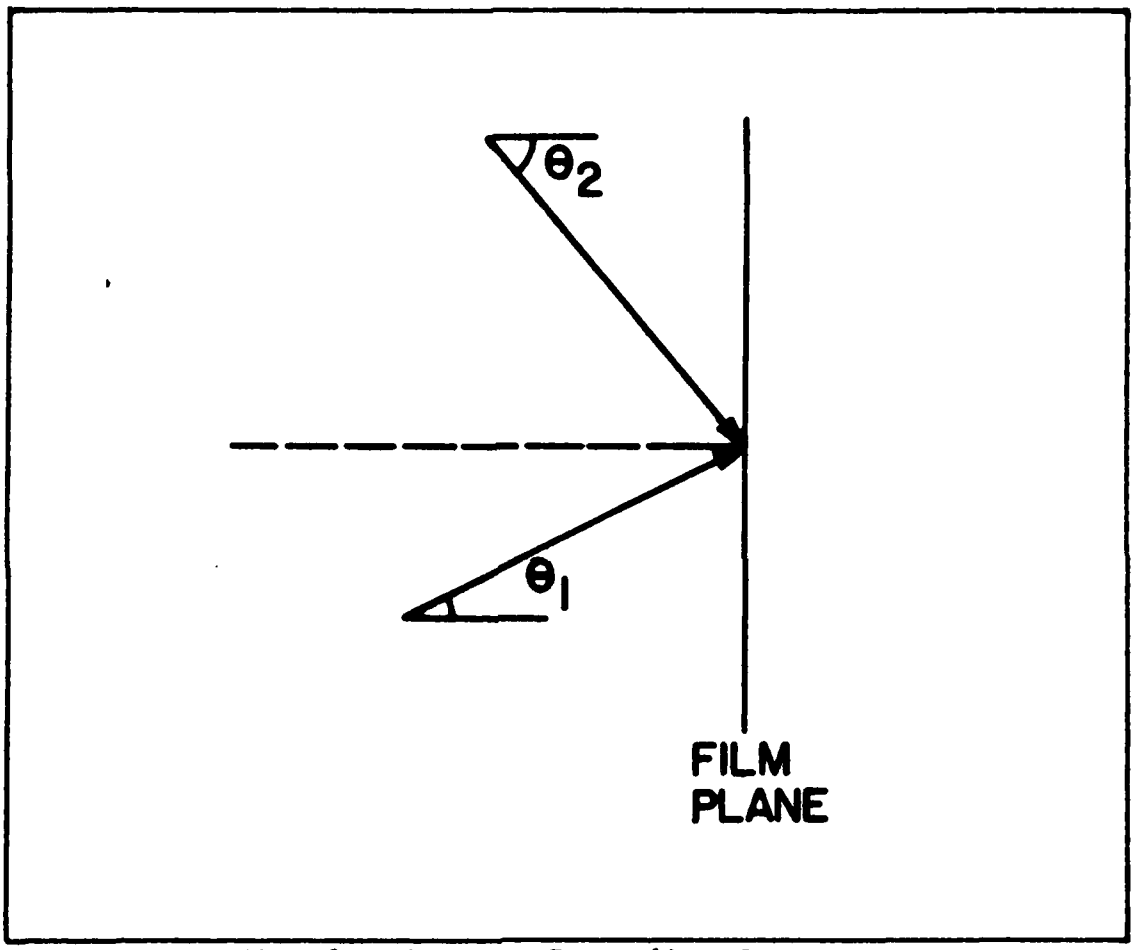

Fig. 1. Grating Recording Geometry

in air is $\lambda_o/2$.

Our diffraction gratings were made by using the experimental setup shown in Fig. 2. Laser light is coherently split into two equally intense beams by a variable beam splitter (BS). After reflecting from carefully placed steering mirrors (M), each beam is then spatially filtered using a microscope objective and pinhole assembly (SF). Finally, f/3.5 lenses (L) are used to collimate the beams before recombination at the film plane (F).

During exposure, an absorptive backing plate is index matched to the back of the recording plate to prevent spurious reflections. Study[24] has shown that a density of 1.7 maximizes absorption by the backing plate. Multiple reflections occur if the density is either too small or too large. When only a portion of each beam is to be recorded, an aperture is placed immediately in front of the recording plate.

To prevent motion of the interference fringes during exposure, all optics are mounted rigidly to a massive steel table using magnetic bases. This includes the film holder which is supported by a damped rod for additional vibration isolation. To minimize vibrational transfer from the laboratory to the table, the massive table is supported by a cushion of air (inflated truck-tire innertubes). These precautions are necessary because vibration of any of the optical components must not exceed a small fraction of a wavelength during the 38 second exposure required for

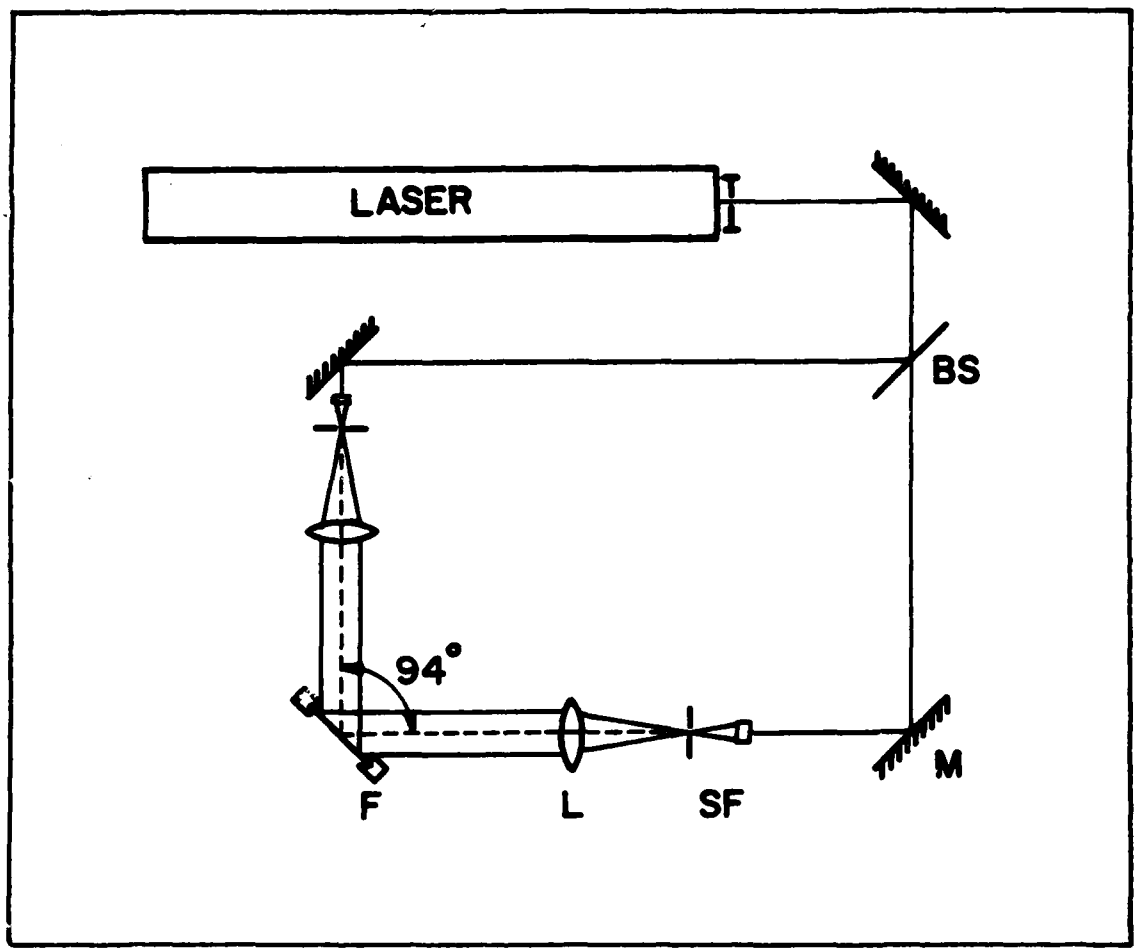

Fig. 2. Experimental Setup used to make Photoresist Gratings

photoresist (at 488 nm). Failure to provide this necessary stability results in a blurring of the fringes, an increase in developer attack rate in so-called unexposed areas, and a subsequent reduction in grating diffraction efficiency.

Additional Experimental Precautions

In addition to the above precautions, the peculiarities of photoresist, especially its insensitivity to visible light, and the difficulties associated with making high efficiency diffraction gratings, forced us to take several additional precautions which are briefly listed and discussed in this section.

For example, even after taking all of the above precautions, unacceptable vibrations may still exist. This proved to be the case in our research. With our laboratory located on the third floor and construction of a new building progressing nearby, daytime exposure proved futile. However, good results were obtained between 12 AM and 6 AM. Thus, in extreme cases, it may be necessary to limit exposure to certain portions of the day or week.

Air-borne disturbances, both acoustic and thermal, can also prove troublesome due to the high laser power and long exposure times required by photoresist. Thus, it is often necessary to turn off or block air-conditioning and ventilation units and to remove or block nonessential sources of heat immediately before and during holographic exposure[23].

We solved this problem by enclosing the optical paths with materials such as cardboard boxes. For best results, the box interiors should be painted with flat black paint.

Careful positioning of the plate holder is also essential for optimum results. Fringes are recorded in their ideal vertical orientation when the plate normal bisects the angle between the two beams. However, because some of the light incident on the emulsion is always reflected, due to the index discontinuity between air and photoresist, a plate so oriented reflects light from each beam into the opposite beam. This reflected light is then focused by the collimating lens back onto the pinhole of the spatial filter. At the pinhole, this light is reflected back again to the film plate where it creates a low-frequency standing-wave interference pattern which is recorded superimposed over the desired pattern. The net result is reduced diffraction efficiency. To avoid multiple reflections from the pinholes, the film plate should be tilted until the surface reflections, when focused by the collimating lenses, miss both the pinholes and any other reflective surfaces.

Equally important is the achievement of maximum fringe visibility (Eq. 15). For photoresist gratings, high diffraction efficiency requires deep grooves which can only be obtained if there is a high contrast between bright and dark interference fringes. Maximum fringe visibility is achieved by making the path difference between the two interfering

beams small compared to the coherence length of the light source, and by maintaining the two beams at equal intensity levels (i.e. a beam ratio of 1) and equal polarizations. Some low-absorption beam splitters rotate the polarization of one of the output beams when used in certain configurations. Some mirror reflections can also rotate polarization. Thus, caution is advised. However, the use of higher-loss beam splitters is not the solution. Beam splitters with large absorption coefficients tend to heat and subsequently deform during exposure, leading to a change in the optical path length of one or more of the beams and the shifting or smearing of the interference fringes.

Also, care should be taken to prevent dust from settling on the optics, especially if cardboard or other paper products are used as barriers. Diffraction from a dust particle in coherent light produces an Airy disc pattern which is recorded, superimposed, over the desired fringe pattern and causes reduced diffraction efficiency.

Finally, optics which are smaller than the laser beam, at the point of use, should be avoided. When the edge of an optical element is illuminated, it acts as a source of diffraction which is then recorded and again leads to lower efficiency.

Theoretical Considerations

The above experimental considerations are not the only requisites for success in producing high-efficiency optical elements. In addition, one must satisfy the theoretical requirement that the spatial frequency be increased until all but one diffracted order is evanescent, as shown in Fig. 3.

In general, readout of a grating, as in Fig. 3, produces diffracted waves at angles

$$\theta_N = \sin^{-1}(\sin\theta_{IN} - N\lambda_o f) \tag{17}$$

where N is an integer. Thus, to avoid higher orders ($N < 0$; $N > 1$), grating spatial frequency must typically exceed $1/\lambda_o$ although a slightly higher frequency may be desirable to avoid diffracted waves which propagate within the substrate. For our experiments, $\theta_1 = 47°$ and $\theta_2 = -47°$, so that via Eq. 16, $f = 3\ \ell/\mu m$.

Additionally, if the grating is fabricated with properly chosen duty cycle, thickness, and fringe shape, nearly all incident power is transferred to the single diffracted order so that the zero order can be nearly eliminated, further enhancing grating efficiency. Theoretical discussions of such gratings are given by Moharam and Gaylord[3] where they predict efficiencies greater than 85%. In their method, a surface-relief grating is divided into thin layers parallel to the grating surface. Then, a state variables

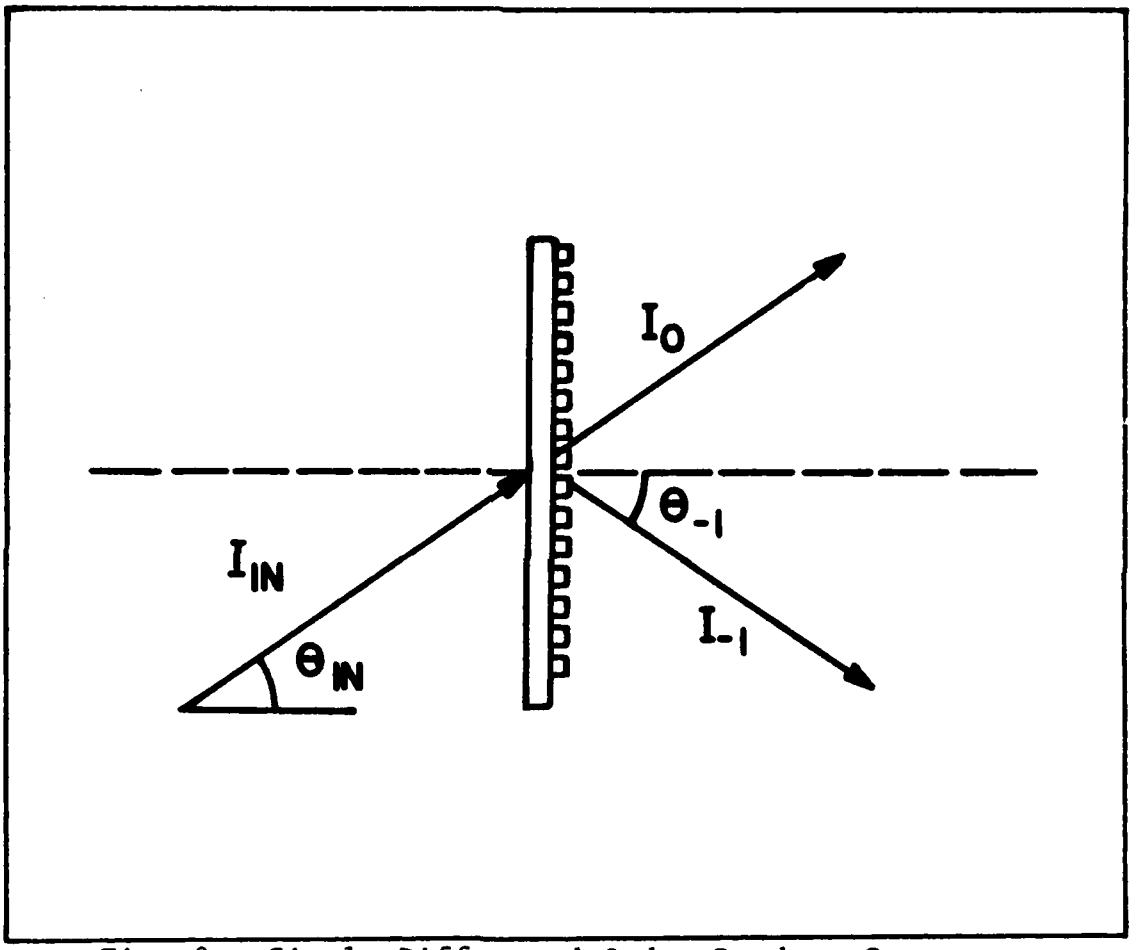

Fig. 3. Single Diffracted Order Readout Geometry

method of solution of the rigorous coupled-wave equations is applied to each layer. With this approach, arbitrary levels of accuracy are possible.

It has long been known that thick volume holograms, for which the index of refraction of the photographic emulsion varies in space, have a theoretical efficiency of 100%[23,25]. Thus, the high efficiencies we have achieved are not so surprising when one realizes that our gratings, even though recorded in films of thickness less than 1 μm, behave as thick gratings. This is because the effective thickness of a grating is characterized by the Q factor[24,26]

$$Q = \frac{2\pi\lambda_o f^2 D}{n} \tag{18}$$

were D is the grating thickness and n is the bulk index of refraction of the film[24]. Typically, if a grating has a Q factor greater than 10, it is considered thick. Since Q depends quadratically on spatial frequency, f, our high frequency gratings appear quite thick. This is further supported by our observation of Bragg effects in the gratings as described later. However, some caution should be used in applying Eq. 18 since volume grating theories are derived by assuming index modulation within the grating is small and energy interchange between the zero and first order takes place over a large distance. Both premises are severely violated for our gratings.

Film Preparation Procedure

Unlike many emulsions, such as Kodak 649F holographic film, photoresist is not commercially available precoated on glass substrates. Thus, before holographically recording gratings, photoresist must first be spin-coated on a glass substrate. We used ultra flat 2x2x0.06 inch soda-lime-silica glass substrates manufactured by Imtec (index of refraction = 1.51).

In preparation for coating, the substrates were cleaned by immersion for 10 minutes in a mixture of 3 parts sulfuric acid to 1 part hydrogen peroxide, followed by a 10 minute wash in flowing DI water. Since the presence of water in the substrate often reduces photoresist adhesion, each substrate was subsequently dried with dry nitrogen gas, baked for 30 minutes at 150° C, and then vacuum baked for another 30 minutes at 130° C.

As soon as the substrates were cool (usually within 10 minutes), they were spin-coated with Shipley AZ-1300 series photoresist. To achieve the photoresist thickness used to make the gratings described in this paper, it was necessary to mix 2 parts AZ-1350B with 1 part AZ-1350J (see Table II). The substrates were flooded with this mixture (a 0.5 μm final filter was used) and then spun at 5500 rpm for 30 seconds. As a final step, the coated plates were baked for 40 minutes at 80° C. This technique produced an after exposure-and-development thickness of approximately 0.62 μm.

(Our research indicates that thicknesses of approximately 0.4 μm are sufficient for high efficiency -- see Chapter IV.)

Exposure and Development

Using the experimental setup shown in Fig. 3, the holographic exposures were made by illuminating each photoresist coated substrate with two plane waves at λ_o = 488 nm. Because photoresist is very insensitive at 488 nm, maximum efficiency required an exposure of 9 J/cm^2, (i.e. an exposure time of approximately 38 seconds).

Shortly after exposure, the photoresist was developed for 35 seconds in AZ developer diluted 1:1 with DI water. This mixture was carefully maintained at 21° since development is very sensitive to both development time and developer temperature. Development was stopped by washing for 1 minute in flowing DI water. The gratings were not postbaked.

Post Development Handling and Processing

Photoresist gratings are very delicate. Any contact with a foreign object will usually cause damage. For example, touching a grating usually abrasively destroys it.

As with all optics, dirt or grease contamination should be avoided. This is especially true for photoresist since it dissolves in acetone (the usual cleaning agent for

optics). In fact, there is essentially no way to clean a photoresist grating aside from blowing off loose particles with a dry gas.

Because of the vulnerability of photoresist gratings, they are sometimes sandwiched between other materials for protection[2]. The photoresist can also be hardened by post-baking. We have successfully postbaked gratings at temperatures up to 120° C without any loss of efficiency. However, according to the Shipley Company, some rounding of the edges of fringes recorded in AZ-1350 photoresist can begin at 120° C, although no measurable movement of fringes should begin until temperatures exceed 130° C. Fringe movement, up to 0.2 μm is possible if temperatures rise to 160° C. Shipley AZ-1350 will be a flowing liquid if heated to 180° C[19].

IV. Properties of High-Frequency Photoresist Gratings

In this chapter we provide the results of detailed measurements of the diffraction properties of our high-frequency gratings. We also compare these measurements to similar ones made on two other gratings: a slightly higher-frequency surface relief grating we made, and a lower-frequency photoresist grating supplied by the Minnesota Mining and Manufacturing (3M) Company.

Measurement Apparatus

The readout geometry used to make grating measurements is shown in Fig. 4. A wedge prism is used on the back

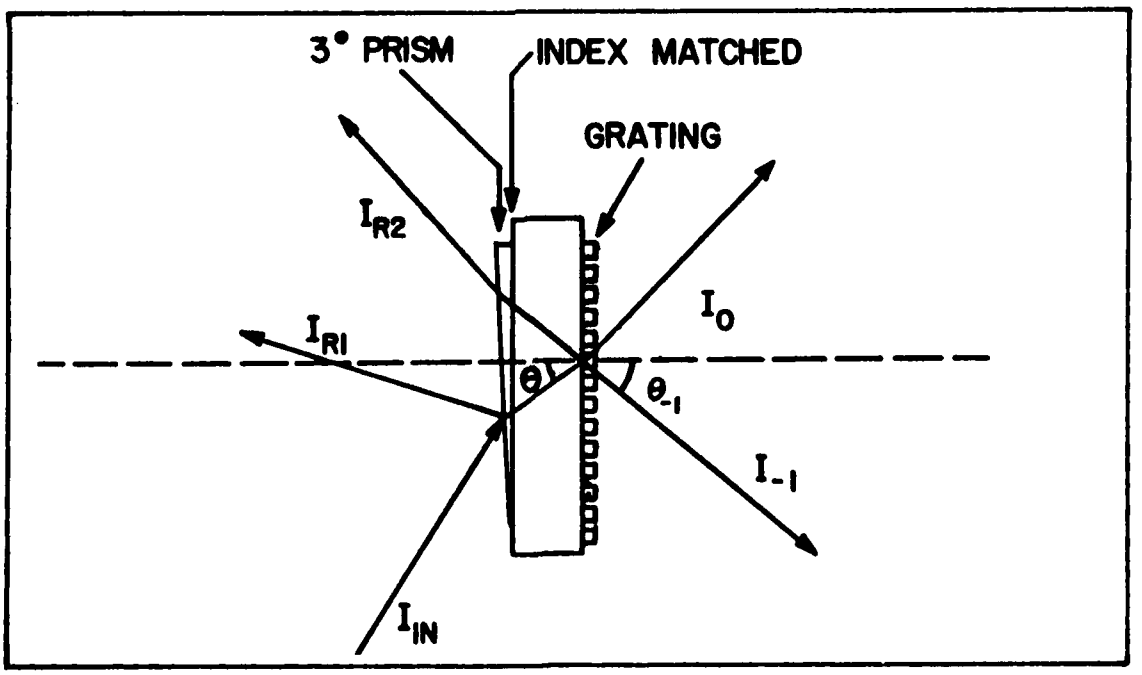

Fig. 4. Actual Readout Geometry Used to Make Measurements

surface of the grating substrate both to distinguish between the various surface reflections and to allow a larger range of readout angles. As shown, the readout angle, θ, is the angle between the incident light (inside the glass substrate) and the glass-resist interface normal, determined experimentally by using Snell's law and the measured angle at the air-prism interface.

Experimental Results

Figures 5 and 6 demonstrate the relationship between the 0 and -1 transmitted orders as a function of θ. They show the ratios I_o/I_{IN} and I_{-1}/I_{IN} as defined in Fig. 3. The I_{-1}/I_{IN} curves have finite angular extent because in Fig. 5, for example, the diffracted wave first appears for $\theta \cong 17°$. Measurements at $\theta > 40°$ were stopped when the width of the incident beam illumination on the grating exceeded the width of the grating, thus making further measurements unreliable. Figures 5 and 6 were obtained using the 476.5 nm line of an Argon laser and 580 nm light from a dye laser, respectively. Note that the peak of the -1 order occurs at a larger incident angle for 580 nm than for 476.5 nm. This is consistent with the fact that our gratings appear to obey Bragg's Law, with the -1 order peaking at the Bragg angle given mathematically by

$$\theta_B = \sin^{-1}\left(\frac{\lambda_o}{2nd}\right) \tag{19}$$

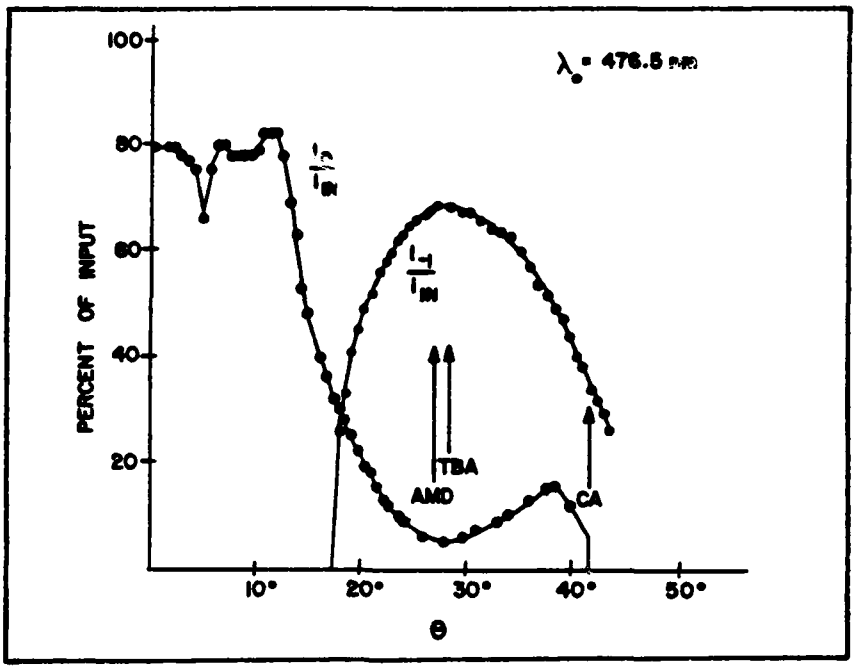

Fig. 5. Relative Intensity vs. Incident Angle
Key: AMD = Angle of Minimum Deviation
TBA = Theoretical Bragg Angle
CA = Critical Angle

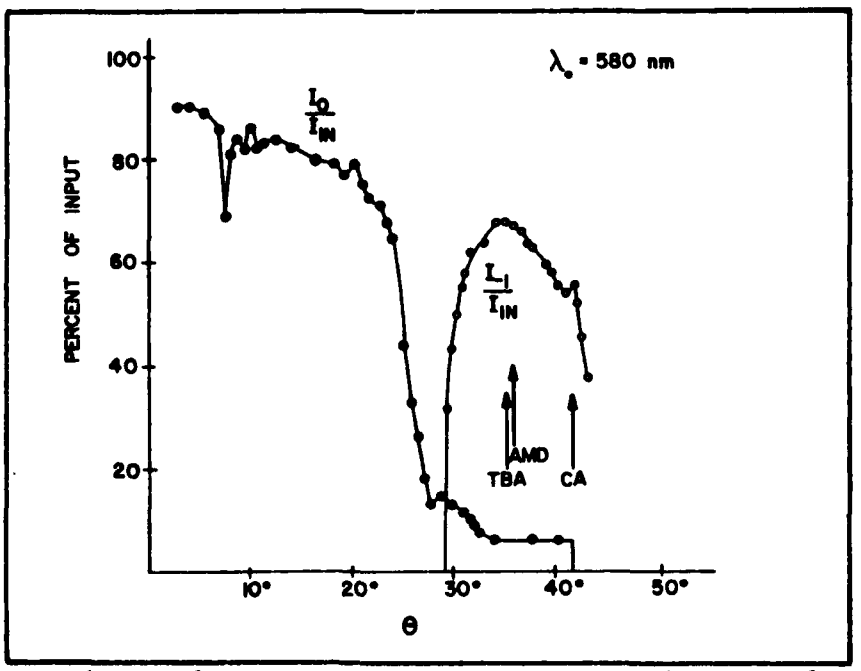

Fig. 6. Relative Intensity vs. Incident Angle

where n is the index of refraction of the glass substrate (1.51), d is the grating spatial period (0.333 μm), and θ_B is defined inside the glass substrate. Thus, at 476.5 nm, $\theta = 28°$ while at 580 nm $\theta = 35°$, both in good agreement with our experimental results.

This correspondence between the -1 order peak and the Bragg angle is somewhat surprising since our gratings are surface-relief gratings. Such correspondence is common among thick gratings (3 μm or more) made in dichromated gelatin where variations in the index of refraction of the exposed and developed gelatin act as Bragg planes just as atoms do in a crystal lattice[27,28]. However, our gratings are at most 0.62 μm thick.

Of course, the actual emulsion thickness is less important than the effective thickness determined by the Q factor. Using Eq. 18, the Q factor for our grating is 13.3 at 476.5 nm and 16.2 at 580 nm where we assumed n = 1.32. To arrive at this value for n we noted from scanning electron microscope (SEM) photographs that our gratings have 50% duty cycles and thus assumed that 50% of each grating has index 1.0 and 50% has index 1.64 (Shipley AZ-1350B). Since our grating Q factors exceed 10, it is possible that the grating fringes are acting as Bragg planes, just as the planes of index variation do in volume holograms.

Note that the maximum irradiance of the -1 order is roughly the same at both wavelengths although the I_{-1}/I_{IN}

curve of the grating is narrower at 580 nm. This narrowing of the diffraction curve at 580 nm results from the large spatial frequency, f, of our grating. At both wavelengths the -1 curves end at roughly the same angle, θ. However, due to the large grating spatial frequency, θ must be larger at 580 nm than at 476.5 nm before the -1 order can emerge (see Eq. 17).

Also note that at small angles of incidence, θ, the 0 order is generally weaker at 476.5 nm than at 580 nm. This is because the grating spatial frequency is still too low at 476.5 nm to prevent the propagation of guided waves (diffracted waves within the substrate) at small angles of incidence). These guided waves rob energy from the 0 order as can be seen by comparing Figs. 5 and 6 between 0° and 20°. The irregularities in the 0 order curves in Figs. 5 and 6, especially those at $\theta = 5°$ and $\theta = 7.5°$, respectively, result from the reflective nature of the grating.

Figures 7 and 8 contain graphs for 476.5 nm and 580 nm, respectively, showing the interaction between the grating's normalized reflective (I_{R2}/I_{IN}) and transmissive (I_{-1}/I_{IN}) diffraction properties. The most notable characteristic is the dramatic rise in grating reflectivity just before the -1 order emerges. Again, this phenomenon is clearly wavelength sensitive. At 580 nm the grating performs nearly as well in reflection as it does in transmission. Also, although the curves become increasingly narrow with wavelength

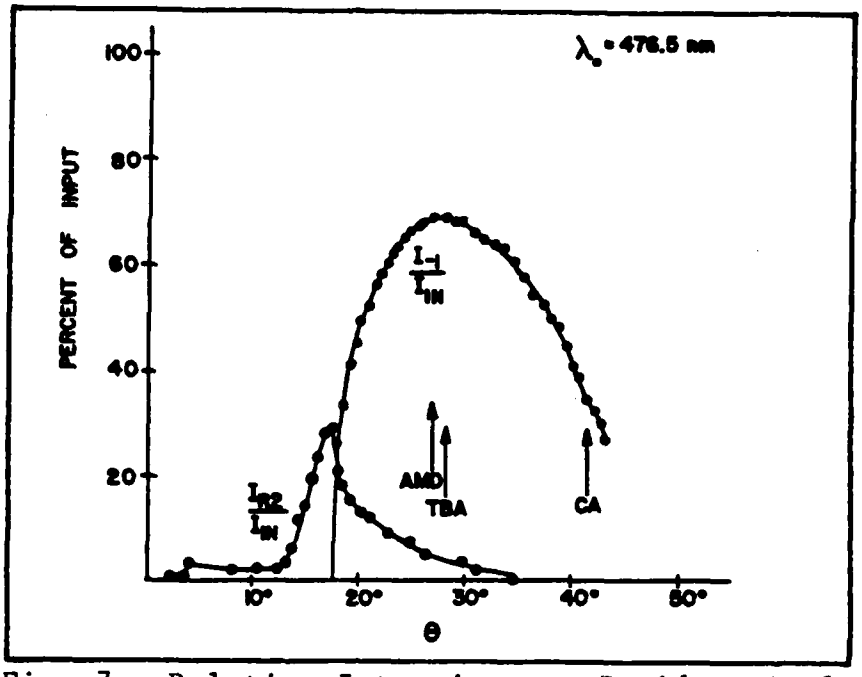

Fig. 7. Relative Intensity vs. Incident Angle

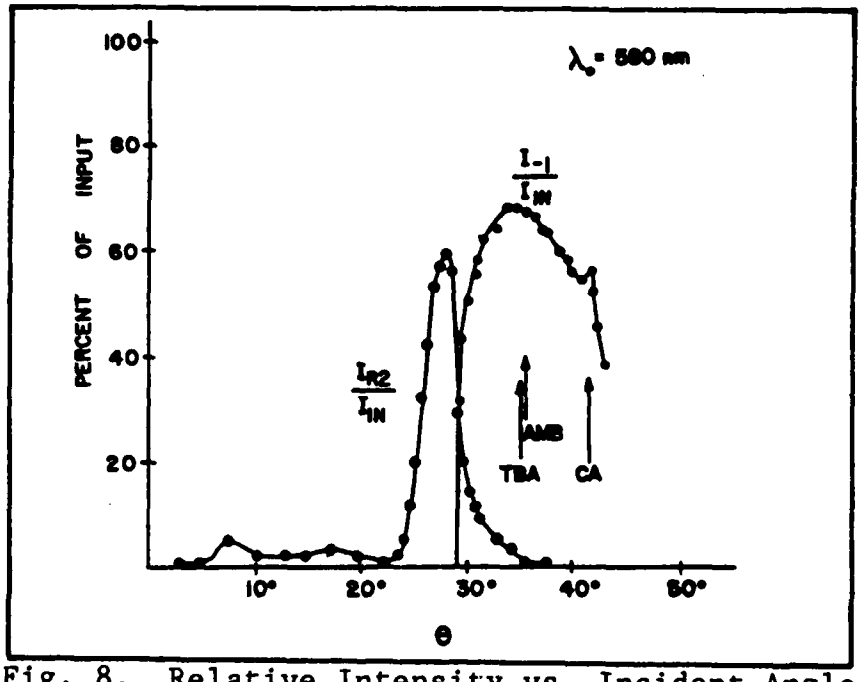

Fig. 8. Relative Intensity vs. Incident Angle

in reflection just as they do in transmission, in both cases the reflection curves are narrower than the transmission curves.

Figures 9 through 12 show the grating efficiency, η, as a function of incident angle at the glass/resist interface for a variety of wavelengths and a larger range of incidence angles. Here

$$\eta = \frac{I_{-1}}{I_{IN} - I_{R1}} \tag{20}$$

The light reflected from the air/prism interface, I_{R1}, has been subtracted from I_{IN} since this surface could be AR coated.

Data displayed in Figures 9 through 12 were collected using the measurement configuration shown in Fig. 4 with the exception that a right angle prism was substituted for the wedge prism. The purpose of the right angle prism was to reduce reflection losses at the air/prism interface for large incidence angles, and to reduce the spot size of the incident radiation (since our gratings have finite size). Both of these effects are severe at large angles of incidence. The right angle prism also enabled us to make measurements at angles of incidence, θ, greater than 42°.

Figures 9 through 12 illustrate an interesting feature of holographic diffraction gratings in photoresist. Note that the angles, θ, corresponding to maximum efficiency are no longer always at the Bragg angles given by Eq. 19.

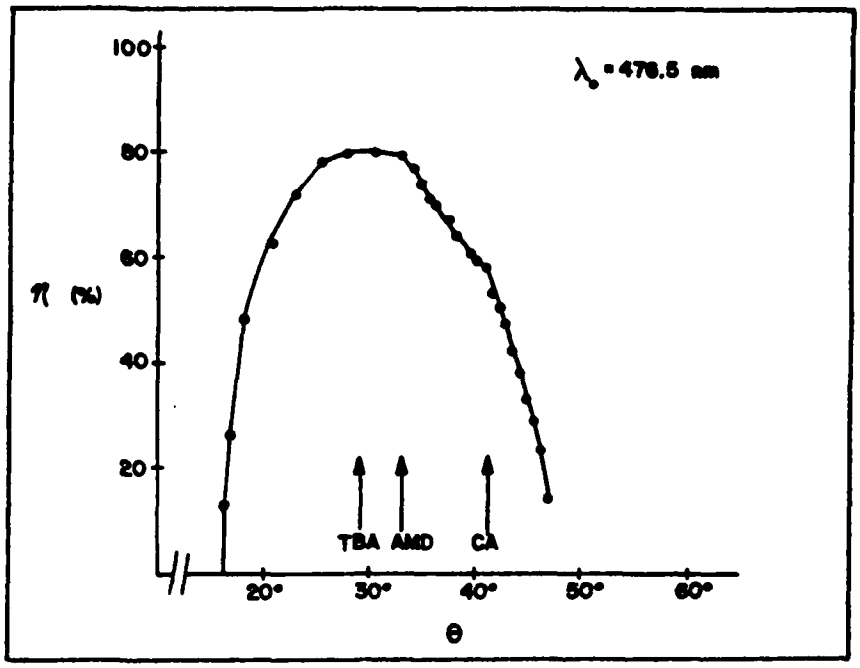

Fig. 9. Grating Diffraction Efficiency vs. Incident Angle--Photoresist

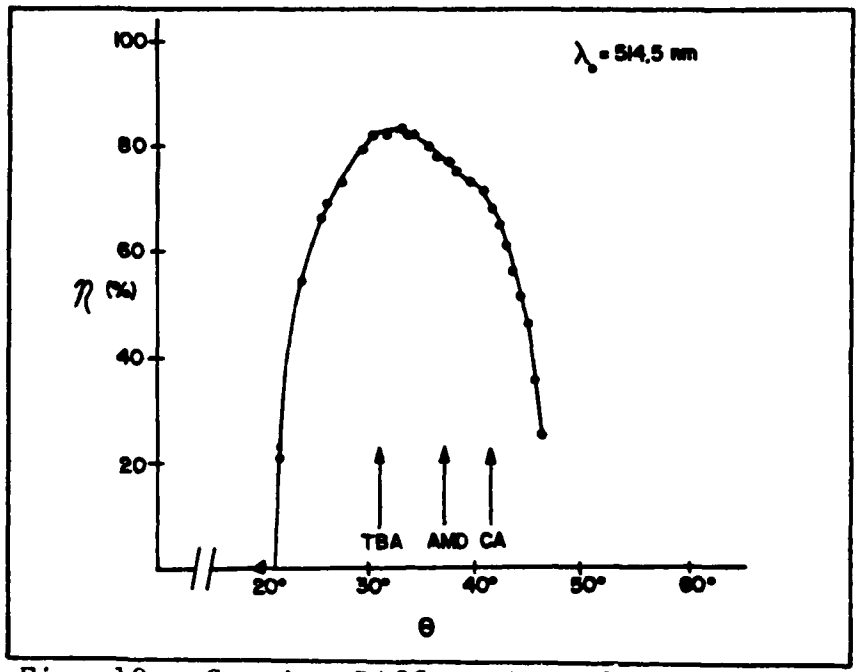

Fig. 10. Grating Diffraction Efficiency vs. Incident Angle--Photoresist

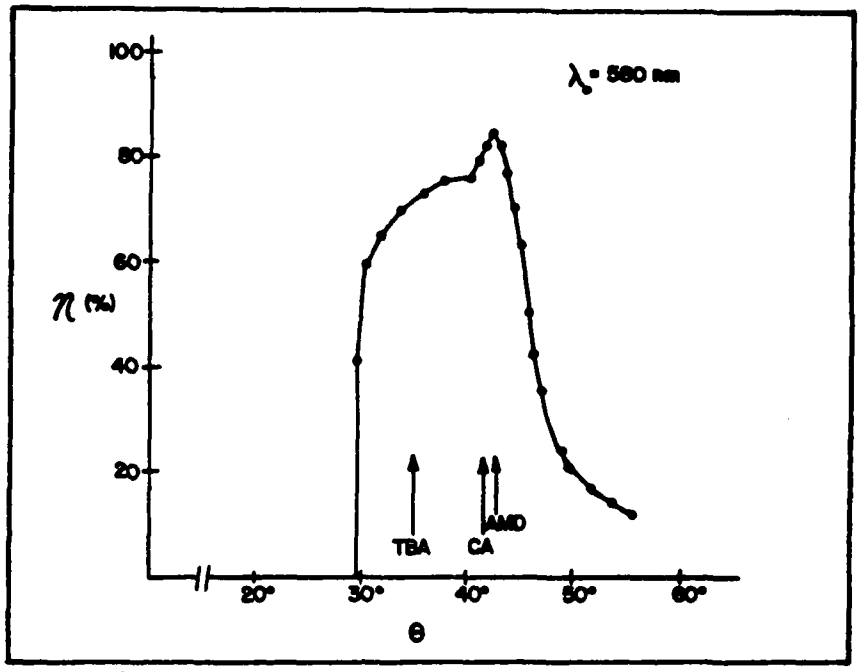

Fig. 11. Grating Diffraction Efficiency vs. Incident Angle--Photoresist

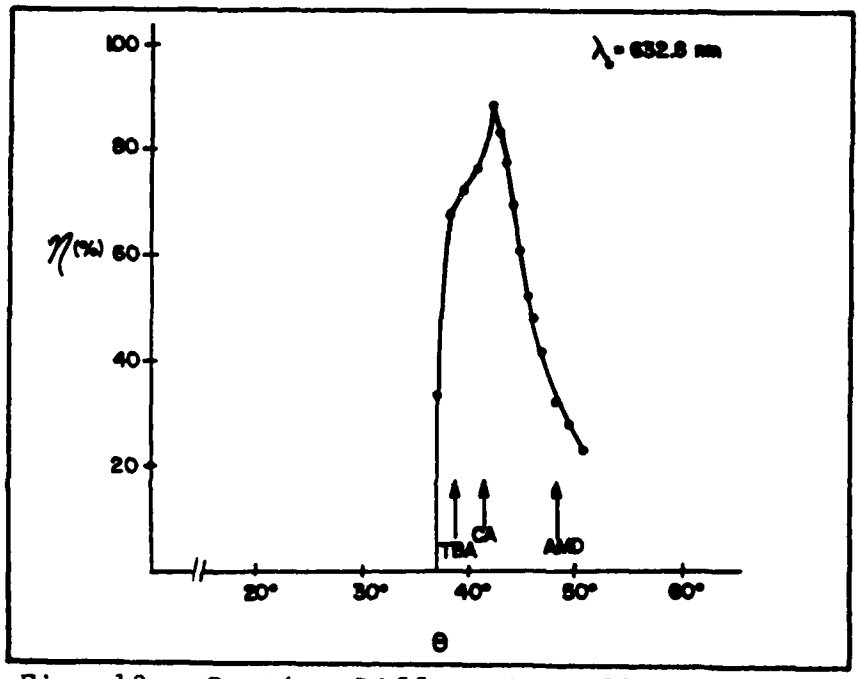

Fig. 12. Grating Diffraction Efficiency vs. Incident Angle--Photoresist

Table III
Angularly Related Properties of Photoresist Gratings

(Wavelength)	TBA (Theoretical Bragg Ang.)	AMD (Ang. of Min Deviation)	Ang. of Max Efficiency
476.5 nm	28.3°	33.2°	30.5°
514.5 nm	30.8°	37.1°	32.5°
580.0 nm	35.2°	42.1°	42.0°
632.8 nm	39.0°	48.6°	42.0°

Table III lists the theoretical Bragg angle (TBA) for our grating, the experimental Bragg angle (obtained by finding the angle of minimum deviation (AMD) for our unslanted grating), and the angle of maximum diffraction efficiency. The glass substrate has an index of 1.51. Note that although the angle of maximum diffraction efficiency is greater than the theoretical Bragg angle (at n = 1.51) in all cases, the effect is most pronounced at longer wavelengths.

In addition, note in Figs. 11 and 12 that the maximum diffraction efficiency at both 580 nm and 632.8 nm occurs at the apex of a sharply rising spike near the critical angle of the glass substrate in air. This result is consistent with a phenomenon reported by Nassenstein[29] and Lee and Streifer[30]. They found that diffraction efficiency is maximized when the reconstruction beam angle is equal to the critical angle. Both articles present curves which closely

resemble the sharply peaked diffraction efficiency curves of Figs. 11 and 12.

Figures 9 through 12 illustrate the significant impact of the critical angle on the efficiency of our photoresist gratings. At the critical angle in Figs. 9 and 10, there is only a slight rise in the grating efficiency. However, in Figs. 11 and 12 there is a large increase in efficiency near the critical angle. Also, note that the angular difference between the theoretical Bragg angle (TBA) and the critical angle (CA) is larger in Figs. 9 and 10 than it is in Figs. 11 and 12. Thus, it appears that when the Bragg angle and the critical angle are sufficiently close, the diffraction efficiency is sharply enhanced, with that enhancement occurring at or near the critical angle. The implication is that the efficiency of photoresist transmission gratings can be significantly enhanced by adjusting the spatial frequency of the required grating device so that the Bragg angle and readout angles both occur near the critical angle.

We note here that when using a high-frequency diffraction grating, illumination of the grating at the critical angle (inside the glass substrate) is useful for laboratory and industrial applications. Were no grating present, light incident at the critical angle would emerge into air at an angle of 90 with respect to the glass normal. However, with one of our gratings, visible light incident at the critical angle in glass emerges in air at angles between

-25° and -64° (see Fig. 4 and Eq. 17). These angles are useful in numerous applications.

The impact of the critical angle can be further illustrated by considering the performance of another grating with a different spatial frequency. Figures 13 through 15 show the grating efficiency, η, as a function of incident angle, θ, at the glass/resist interface for a quartz surface-relief grating made as described in Chapter V. By measuring the angle at which the first order emerges, and by using Eq. 16, we determine that the grating has a spatial frequency of 3.05 $\ell/\mu m$ (grating spatial period of 0.328 μm compared to 0.333 μm for our photoresist grating). As with our photoresist grating, measurements were made using the configuration shown in Fig. 4 with a right angle prism substituted for the wedge prism.

Comparing Figs. 15 and 11, note that the diffraction efficiency is markedly enhanced at 580 nm for the quartz grating; more so than for our slightly lower frequency photoresist grating. Also, comparing Figs. 14 and 10, obvious enhancement at 514.5 nm is apparent for the quartz grating while it is barely noticeable for our photoresist grating. These results are not surprising since the theoretical Bragg angle given by Eq. 19 is inversely related to grating spatial period (directly related to spatial frequency). Thus, for a given wavelength, the theoretical Bragg angle and critical angle are slightly closer for our

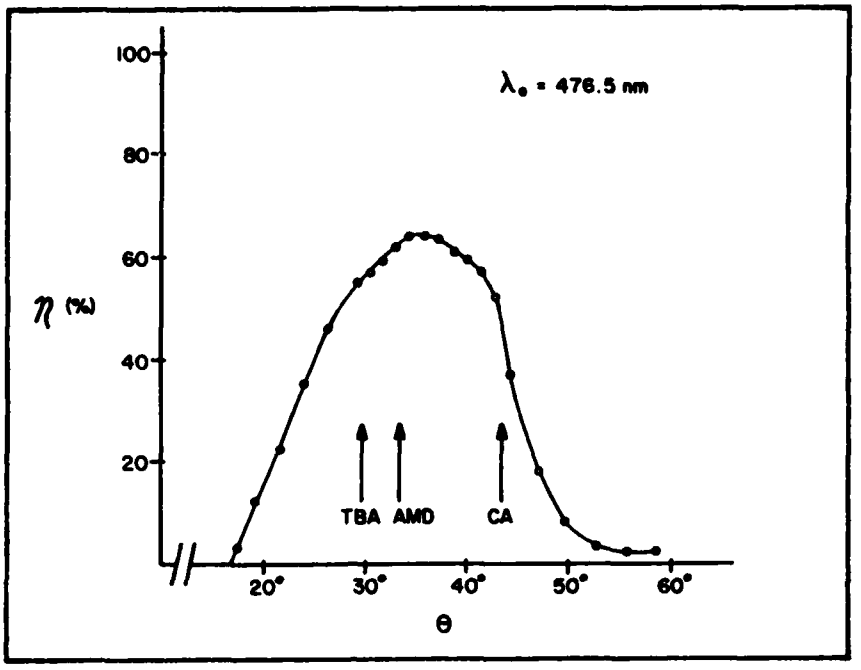

Fig. 13. Grating Diffraction Efficiency vs. Incident Angle--Quartz Grating

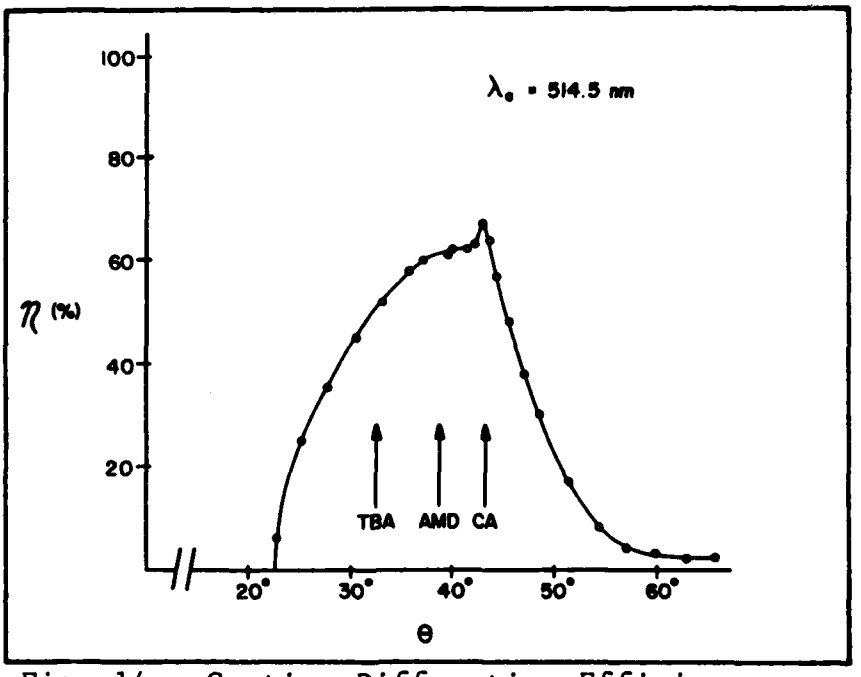

Fig. 14. Grating Diffraction Efficiency vs. Incident Angle--Quartz Grating

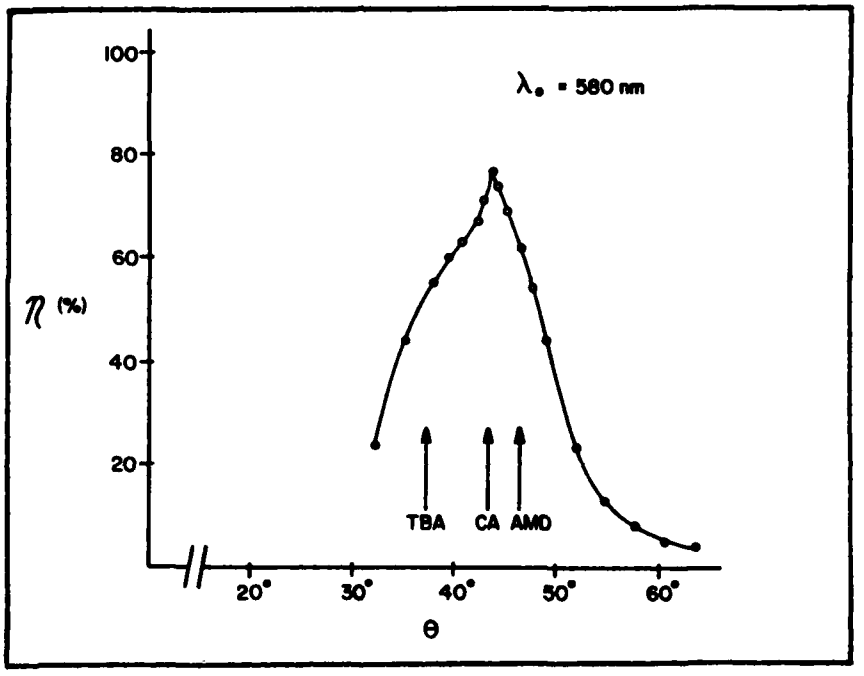

Fig. 15. Grating Diffraction Efficiency vs. Incident Angle--Quartz Grating

quartz grating than for our photoresist grating. If efficiency enhancement depends on the proximity between theoretical Bragg angle and critical angle, then the greater enhancement at 514.5 nm for the higher frequency quartz grating is reasonable.

Unfortunately, the theory relating theoretical Bragg angle, critical angle, and diffraction efficiency enhancement does not appear to be as direct as the above discussion implies. To illustrate this, consider Figs. 16 through 20 which show the results of efficiency measurements made with the 3M photoresist grating. Using measurements of first order emergence and Eq. 16, the calculated spatial frequency of this grating is 2.27 ℓ/μm. Again, efficiency measurements were made using the setup shown in Fig. 4 with a right angle prism substituted for the wedge prism.

Note that the efficiency of the 3M grating is enhanced near the critical angle, just as is the efficiency of our two other gratings. Also, just as with our other gratings, the enhancement of efficiency near the critical angle diminishes, and even seems to disappear, when the theoretical Bragg angle and critical angle are far enough apart (in terms of θ). However, the 3M grating displays more enhancement at shorter wavelengths than do ours. This is somewhat surprising since the theoretical Bragg angle for a given wavelength is smaller for the 3M grating than for ours. If efficiency enhancement depends solely on the proximity

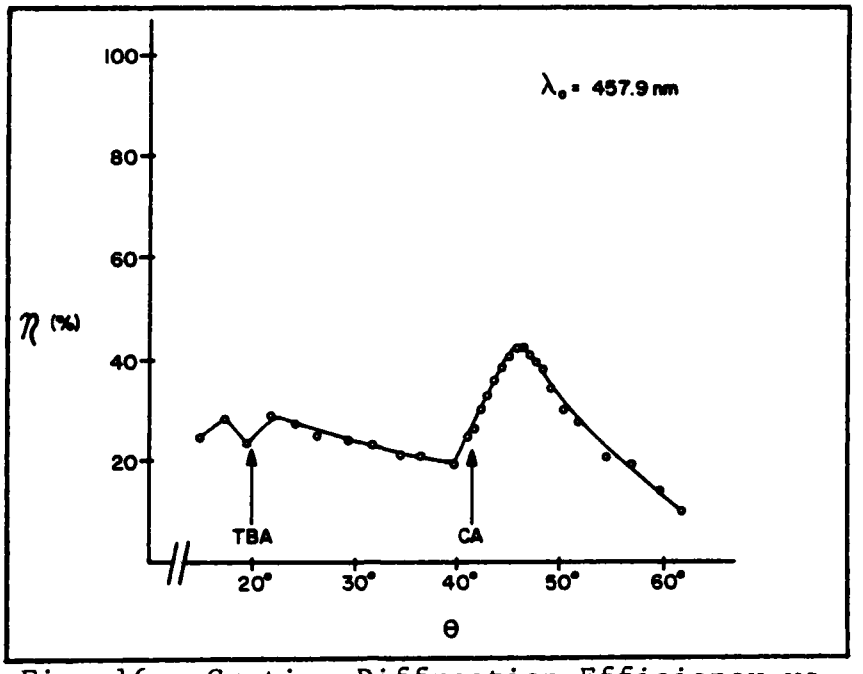

Fig. 16. Grating Diffraction Efficiency vs. Incident Angle--3M Grating

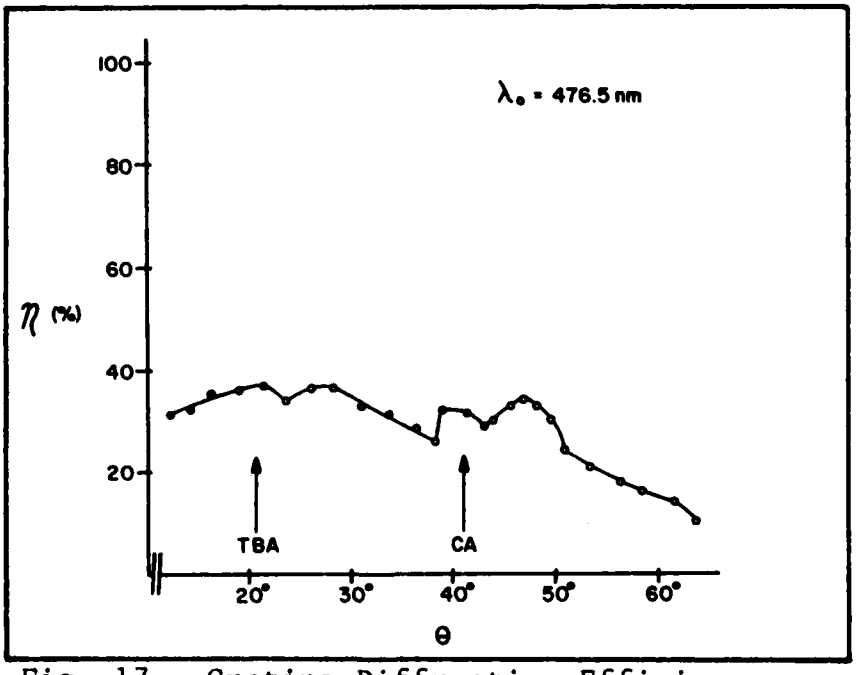

Fig. 17. Grating Diffraction Efficiency vs. Incident Angle--3M Grating

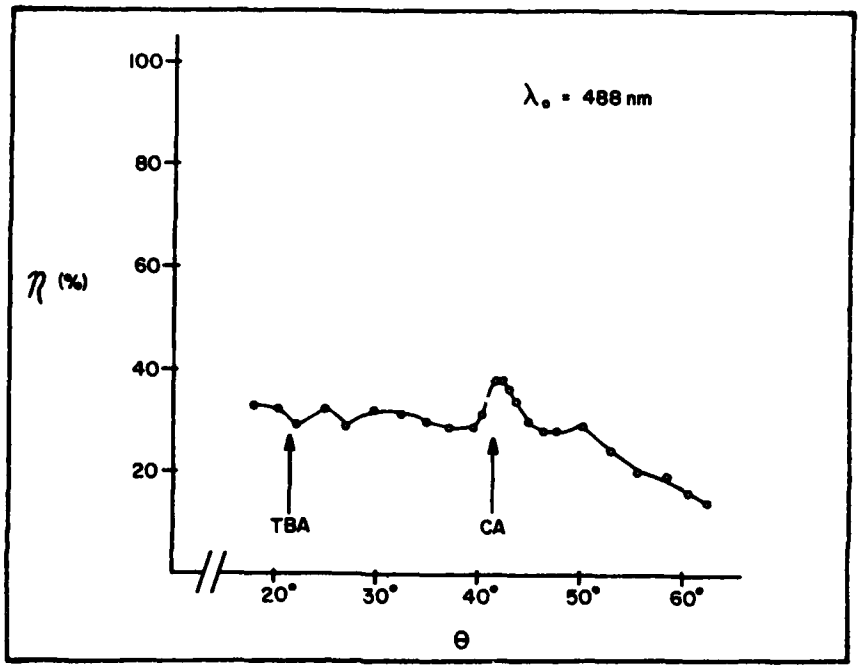

Fig. 18. Grating Diffraction Efficiency vs. Incident Angle--3M Grating

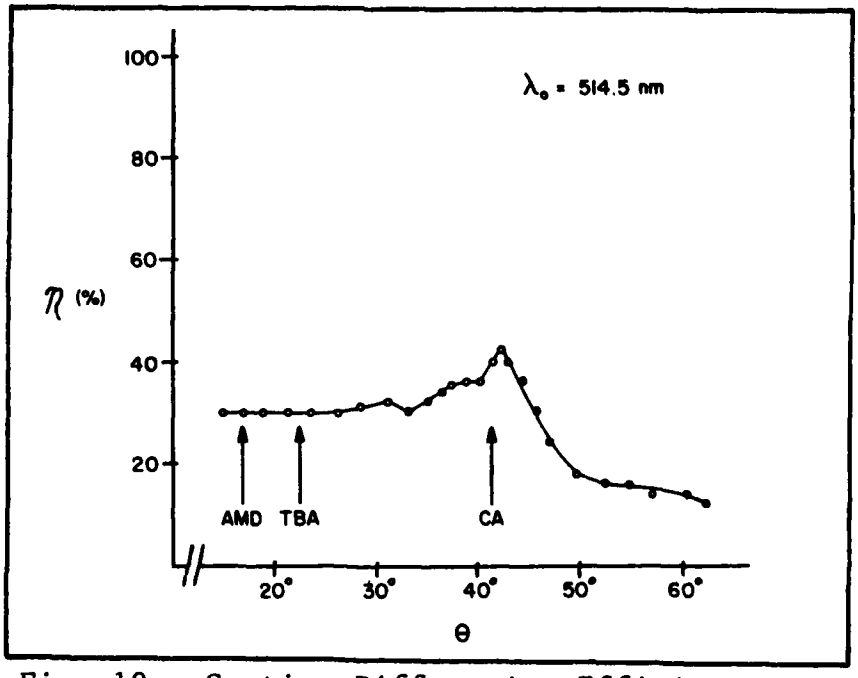

Fig. 19. Grating Diffraction Efficiency vs. Incident Angle--3M Grating

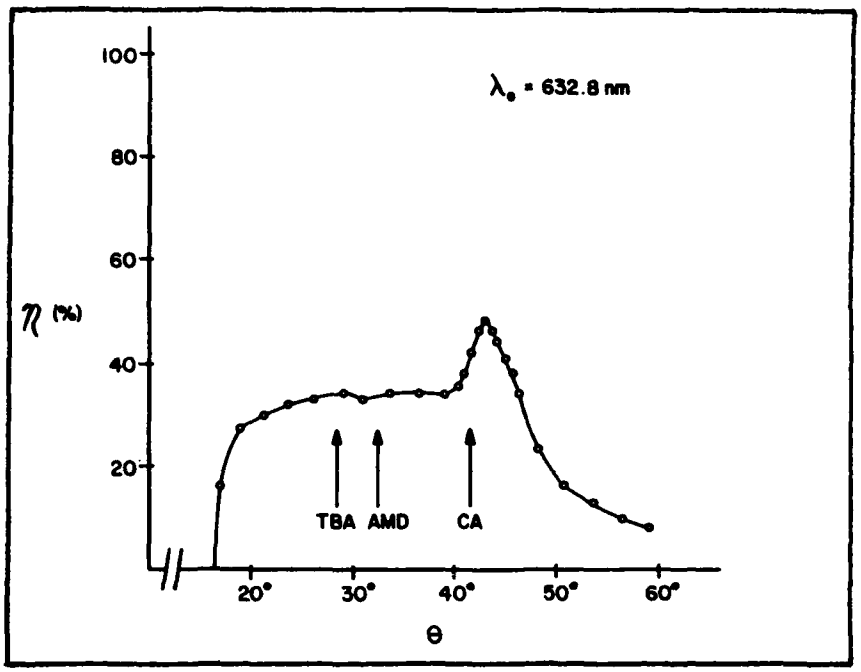

Fig. 20. Grating Diffraction Efficiency vs. Incident Angle--3M Grating

between the theoretical Bragg angle and critical angle, then the 3M grating, with a smaller Bragg angle at each wavelength, should display efficiency enhancement only at longer wavelengths.

Another notable feature of the 3M grating concerns periodicity. Figures 16 through 20 suggest that efficiency enhancement near the critical angle is periodic, perhaps in terms of multiples of the Bragg angle. Consider Figs. 16 through 20 in reverse order (i.e. in order of decreasing wavelength). The most significant enhancement occurs at 632.8 nm (Fig. 20). This enhancement decreases with decreasing wavelength until in Fig. 17 it seems to disappear entirely. Simultaneously, a seemingly new peak first appears in Fig. 18 at $\theta = 50°$. In Fig. 17 this peak increases and occurs at $\theta = 47°$, shifted slightly towards the critical angle. Finally, in Fig. 16 the peak is even more pronounced and has shifted even closer to the critical angle while simultaneously a small efficiency enhancement has begun to appear at the critical angle. Perhaps, if shorter visible wavelengths were available, we would find that this peak eventually becomes localized near the critical angle, having come full cycle from the observed result at 632.8 nm.

Although all of the interactions are not clear, it does appear that, as we observed with our gratings, the diffraction efficiency is sharply enhanced when the theoretical Bragg angle and critical angle are sufficiently close.

However, the results of our study of the 3M grating suggest that the effect is most likely more complicated than that, depending on more variables than just the proximity of the theoretical Bragg and critical angles. While a definitive answer to this problem may be of importance to grating designers, further pursuit of this question is beyond the scope of this thesis.

Figures 21 through 23 are graphs of peak efficiency as a function of illumination wavelength for the three gratings evaluated in this chapter.

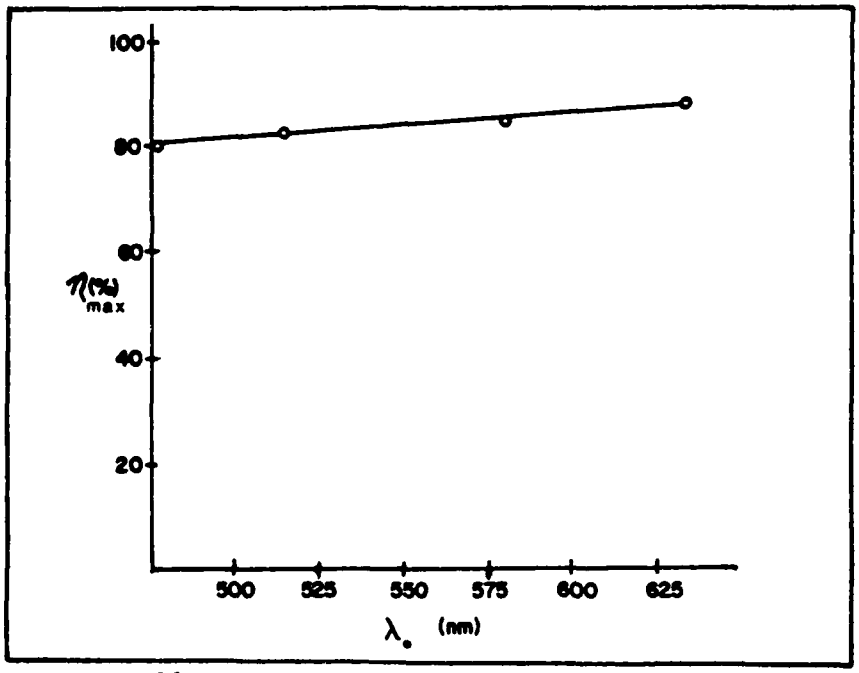

Fig. 21. Maximum Grating Efficiency vs. Incident Wavelength--Photoresist

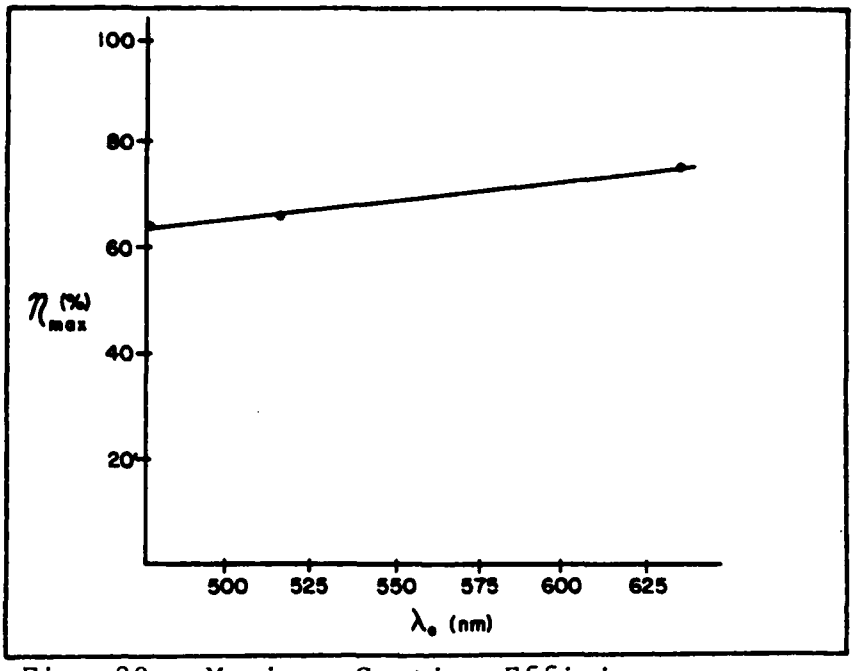

Fig. 22. Maximum Grating Efficiency vs. Incident Wavelength--Quartz Grating

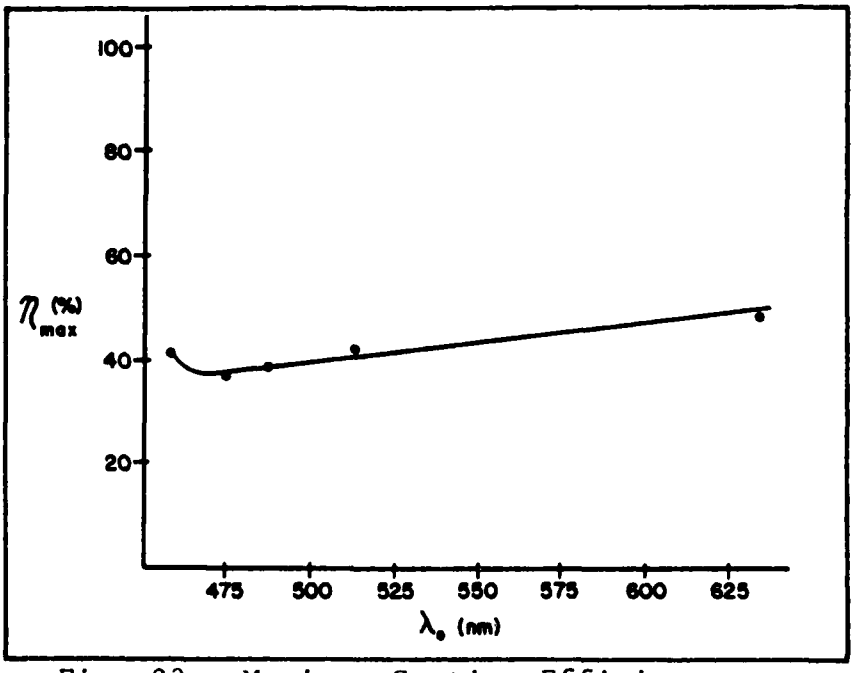

Fig. 23. Maximum Grating Efficiency vs. Incident Wavelength--3M Grating

Figures 21 through 23, as composites of Figs. 9 through 12, 13 through 15, and 16 through 20, respectively, demonstrate that efficiency increases with increasing wavelength although Fig. 23 again suggests that this affect may be periodic, as discussed above.

The high efficiencies obtained in this research result from our ability to produce deep feature sizes in the photoresist. Figures 24 and 25 contain SEM photographs of one of our photoresist gratings. Figure 24 is a top view showing the regularity and clarity of the grating fringes. Figure 25 shows more detail. Note that the fringe depth is approximately 0.37 μm and the spatial period is 0.333 μm so that the depth to period ratio is 1.1, a requirement for high efficiency as predicted in Refs. 2 and 3.

Figures 24 and 25 are evidence that holography can be used to produce very narrow lines in photoresist. Our photoresist gratings have fringes roughly 0.2 μm wide. These narrow lines are of particular interest to the microelectronics industry. In Appendix A we discuss the applicability of holography to the manufacture of integrated circuits.

An Alternative to the Prism

Before closing this discussion of the properties of our high-frequency photoresist gratings, we offer one additional suggestion. Although the exact relationship is unclear,

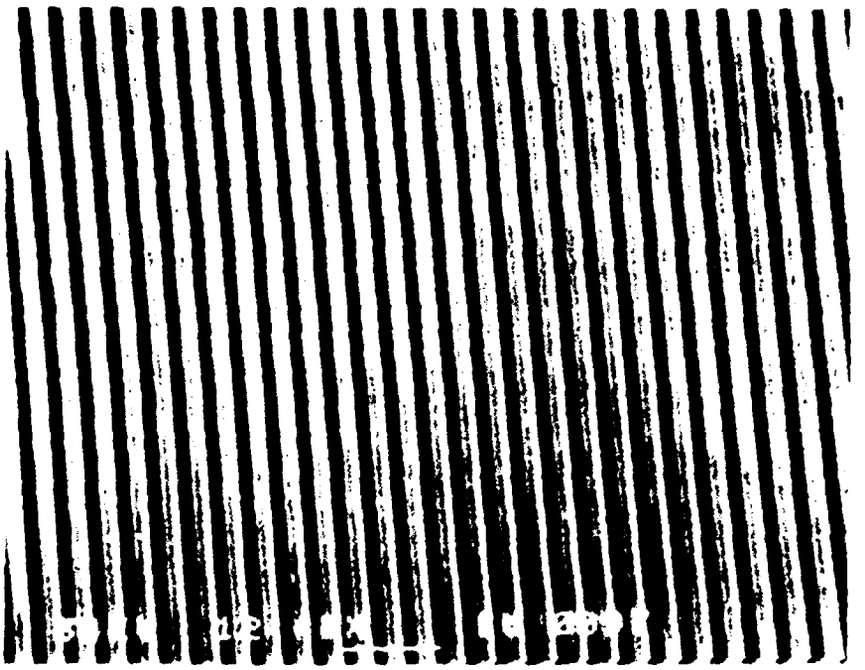

Fig. 24. SEM Aerial View of Photoresist Grating Fringes
Scale: Horizontal Bar at Bottom of Photo Equals 1.0 μm

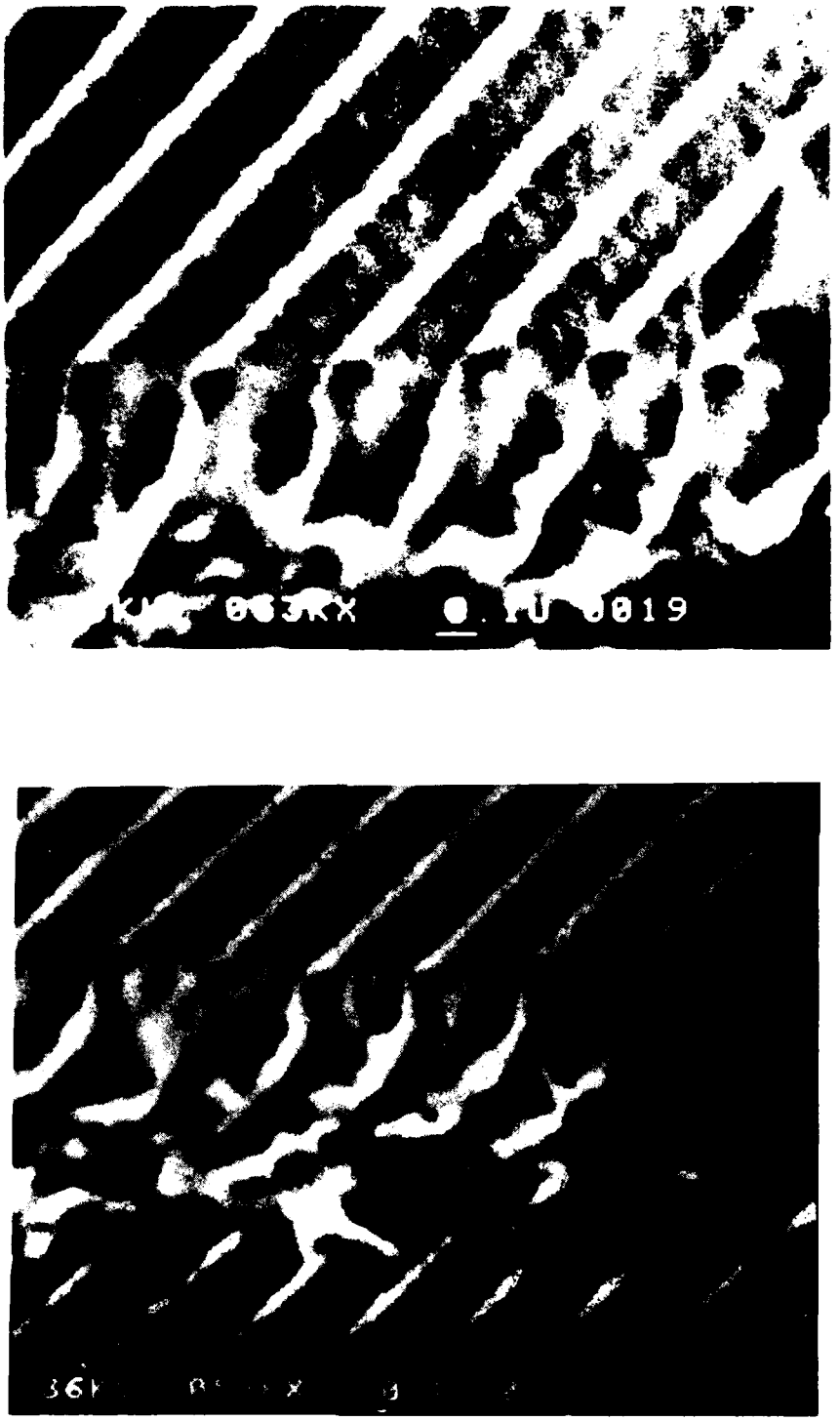

Fig. 25. SEM Photographs of Photoresist Grating.
Profile is Visible Due to Small Scratch in Grating.
Scale: Small Horizontal Bar at Bottom of Each
Photo Equals 0.1 μm.

there is no doubt that the efficiency of these gratings is frequently greater when incident angles, θ, are near the critical angle. Thus, we note that the effect of the critical angle on diffraction efficiency is another strong reason for using a prism when illuminating one of our gratings. Without the prism, light cannot be efficiently coupled into the grating at angles, θ, near the critical angle because of large surface reflection losses. In addition, without a prism, no incident angles, θ, greater than the critical angle can be accessed at all.

Because a prism is important to the achievement of high diffraction efficiency and because prisms are bulky and awkward to use, we offer the following alternative solution which preserves the advantages of the prism but reduces the bulk. If one of our gratings is illuminated from the grating side, any incident angle from -90° to 90° can be accessed. By itself, this method of illumination provides no advantage. Under direct grating illumination the most intense diffracted waves are near the critical angle inside the grating substrate and either exit the back side of the substrate near 90° (measured from the normal) or remain in the substrate as guided waves. However, if the back of the substrate is index matched to the back of another of our gratings, then the diffracted waves from the first grating can enter the second at angles near or greater than the critical angle. Thus, the first grating acts just like a

prism but without the bulk and mass. In an ideal situation, a grating would be applied to each side of a single substrate, further reducing the required bulk and mass, as well as simplifying handling. This technique would be especially advantageous if one of the gratings had focal power or aspheric properties.

We index matched two of our high-frequency photoresist gratings and using 632.8 nm illumination found maximum diffraction efficiencies exceeded 84% just as with a right angle prism. We note that without either a prism or a grating we have never achieved such high diffraction efficiencies because without a prism or grating we are unable to efficiently couple 632.8 nm light into the grating at the required incident angles.

V. Fabrication of Durable High-Frequency Optics

In previous chapters, we have considered the fabrication and diffraction characteristics of Holographic Optical Elements (HOEs). In this and the next chapter we turn to consideration of the potential uses of HOEs.

Background

The primary advantages of HOEs are their light weight, low cost, relative ease of fabrication[31], and capacity to produce complicated wavefronts[32]. However, care must be used in selecting the proper applications for HOEs. For example, HOEs suffer from large chromatic aberration. Additionally, thin elements, until recently, exhibited low diffraction efficiency[33].

Perhaps the best known modern uses of HOEs are in optical element testing[34] and in scanners[1,2]. However, HOEs are also found in beam-waveguide couplers, beam splitters[28], filters[35], polarizers, distributed feedback circuit elements[36] and head-up displays in aircraft cockpits[4]. Although HOEs are sometimes used directly as recorded in their photographic emulsions, some HOEs, such as those made in photoresist, are extremely vulnerable to damage, both abrasive and chemical (see the last section of Chapters II and III). Thus, occasionally the holographically recorded patterns are transferred to the substrate via chemical etching, ion beam bombardment[35,37] or a combination of the

two methods known as reactive ion etching[38]. A variety of substrate materials are used such as GaAs[39,40], SiO_2[41], Au[42], or, as in our case, glass[43] or quartz. In this chapter we discuss the fabrication of these etched optical elements with deeply corrugated optical surfaces. Then, in the next chapter, we discuss two new applications for these optical elements.

Photoresist Mask Processing

In this section we briefly describe the procedures we followed in preparing the photoresist masks needed for reactive ion etching. The general comments pertaining to holographic grating construction in photoresist which are contained in Chapter III still apply. However, the procedures outlined below are different enough from those used for production of our photoresist diffraction gratings that they are included here.

Fused quartz substrates were selected because they have no measurable birefringence and because they are suitable candidates for reactive ion etching. Each substrate was thoroughly cleaned using several baths of acetone, followed by methanol, and finally DI water. Since the presence of water in the substrate often reduces adhesion of the photoresist, each substrate was subsequently dried with dry nitrogen gas, baked for 30 minutes at 150° C, and then vacuum baked for another 40 minutes at 150° C.

As soon as the substrates were cool they were spin-coated with Shipley AZ-1350B photoresist. The substrates were flooded with this mixture, using a 0.2 μm final filter, and then spun at 3000 rpm for 30 seconds. This produced a resist layer approximately 0.4 μm thick[18]. As a final step, the coated substrates were baked for 40 minutes at 80° C.

The holographic exposures were made by illuminating the photoresist coated substrate in the usual way with two plane waves separated angularly by approximately 90°. Using a wavelength of 457.9 nm, a grating with a period of about 0.3 μm was produced. This small period guarantees that all diffracted orders are evanescent under normal incidence (i.e., 0°) illumination, a condition we need for the applications discussed in the next chapter. Following exposure, each photoresist film was developed for 35 seconds in AZ developer diluted 1:1 in DI water. This mixture was carefully maintained at 21° C since development is very sensitive to both development time and developer temperature. Development was stopped by washing for 1 minute in flowing DI water. The gratings were not postbaked.

Reactive Ion Etching

Transfer of the photoresist grating pattern to the quartz substrate was accomplished by CHF_3 reactive ion etching. Specific procedures depend upon the actual machine

used. However, processing holographically-generated diffraction gratings with periods as small as ours does present one additional problem. Figure 25 contains SEM photographs of a photoresist grating similar to the ones prepared as masks in this research. Note that there appears to be some photoresist remaining at the bottom of the deep grooves. We found it virtually impossible to eliminate this residual photoresist. Additional exposure or development led to grating destruction rather than further removal of photoresist in the grooves. The presence of this residual photoresist does not pose a problem if the gratings are to be used without further processing. However, for reactive ion etching this extra material means that the substrate is not directly available for ion attack.

To solve the problem of residual photoresist we did two things. First, we increased exposure times to just before the point where grating degradation would begin. Secondly, just prior to reactive ion etching, we exposed the photoresist grating to an oxygen plasma. A 1 minute oxygen scrub proved optimum. The advantage of the oxygen scrub is that it quickly removes a uniform layer of photoresist, thereby reducing and eventually eliminating the residual photoresist remaining in the grooves. The disadvantage of the technique is that the height of the photoresist peaks is also reduced, thereby reducing the potential depth of the etch. However, in our experience, this disadvantage was more than offset by

the improvements in etch rate and reproducibility resulting from the oxygen scrub.

Following reactive ion etching, excess photoresist still present on the substrate was removed in an oxygen barrel asher. The optical elements are at this point very durable because the substrate itself is corrugated.

Table IV lists the etching parameters used to produce the gratings discussed in this thesis. The high selectivity etch used a different gas mixture designed to increase the etch rate of the quartz relative to the photoresist.

Durability of Etched Gratings

As mentioned above, after etching and oxygen ashing, our quartz gratings are much more durable than our photoresist gratings. Our tests show that the quartz gratings can be washed in solvents such as acetone or methanol without any measurable loss in performance (i.e. in diffraction efficiency or in use in the two applications to be discussed in Chapter VI). In this section we report on tests[44] to determine the durability of our quartz gratings when exposed to intense laser radiation.

Gratings 3, 6, and 7 were selected for testing as a representative sample of the gratings we have made (see Table IV). Because these gratings had been handled extensively during other testing, each grating was cleaned with acetone, methanol, and distilled water before being sent for

Table IV
Quartz Grating Etching Parameters

Grating #	O_2 Plasma	Standard Etch	High Selectivity Etch
1	1 min.	20 min.	
2	1 min.	40 min.	
3	1 min.	40 min.	
4	1 min.	60 min.	
5	1 min.	60 min.	
6	1 min.	90 min.	
7	1 min.	11 min.	79 min.
8	2 min.	90 min.	
9	2 min.	11 min.	79 min.
10	3 min.	90 min.	
11	3 min.	11 min.	79 min.

radiation testing. The actual radiation testing was conducted by Barry Crane and Robert O'Connel at the United States Air Force Academy.

Grating 3 was tested under very controlled conditions using a Quanta Ray Nd YAG laser. The output wavelength was 1006 nm and the full width at half max (FWHM) pulse length (duration) was 9 nsec as measured with a photodiode on a high speed storage scope (1 GHz). During testing, energy per pulse was varied with a cross polarizing prism. Measurements of the energy per pulse were made with a

calorimeter. In each case the beam was focused to a spot of 70 μm in radius.

Table V contains results of testing conducted on grating 3. Flux and fluence measurements were certain within a few percent. For each flux and fluence, several locations (sites) on the grating were tested. Damage percentages represent how many of these sites sustained damage. During testing, damage sites were examined with an interferometer. Phase contrast microscopy, used after testing, revealed the presence of radial cracking in damage sites.

Table V
Damage Resistance to High Power Laser Radiation (1006 nm)
Grating 3

Fluence J/cm^2	Flux GW/cm^2	Results Percentage of Sites Damaged
15.0	1.67	10% Damaged (3 of 30 sites tested)
17.1	1.89	50% Damaged (10 of 20 sites tested)
24.5	2.73	100% Damaged (all of at least 30 sites)

For comparison purposes, clean air breakdown occurs at about 100 GW/cm^2.

In testing grating 3, some test sites received as many as 300 pulses using a 10 Hz repetition rate. Surprisingly, multiple pulses did not change the damage threshold. If the grating failed, it failed on the first pulse.

Grating 7 was tested with the Quanta Ray Nd YAG laser followed by a KD*P frequency doubler. Compared to

grating 3, grating 7 was illuminated with considerably larger beams using full laser power. Normally, larger spots yield lower damage thresholds because the probability of illuminating a fault or imperfection in the grating greatly increases. A lens was used to give several different spot sizes. The energy per pulse was 450 mJ ± 50 mJ with a pulse length of 2 nsec FWHM. Results of the testing are contained in Table VI.

Table VI
Damage Resistance to High Power Laser Radiation (503 nm)
Grating 7

Fluence J/cm^2	Flux GW/cm^2	Spot Size cm^2	Results
1.17	0.585	0.385	No Damage for 3 sites
2.83	1.41	0.16	No Damage for 3 sites
6.37	3.2	0.071	No Damage for 3 sites
57.3	28.6	0.0078	100% Damage

The results of testing done on grating 6 are contained in Table VII. This time the laser was used without the second harmonic generator. Approximately 800 mJ pulses were used with pulse lengths of 4 nsec FWHM. A lens was again used to decrease the spot size.

Table VII
Damage Resistance to High Power Laser Radiation (1006 nm)
Grating 6

Fluence J/cm^2	Flux GW/cm^2	Spot Size cm^2	Results
2.08	0.52	0.385	No damage for 3 shots
8.32	2.08	0.096	No damage for 3 shots
16.3	4.17	0.049	No damage for 3 shots
50	12.75	0.015	100% damage

As a result of the testing, Crane, who has done extensive testing on the damage thresholds of diffractive optics, draws the following conclusions regarding our quartz gratings[44]:

"1. The grating could be routinely operated with normal cleaning at full power of the best Quanta Ray DCRs. No commercial gratings can operate under these conditions....

"2. Large spot sizes usually yield significantly lower damage thresholds. This does not appear to be the case with these gratings.

"3. High repetition rates do not degrade the grating--up to 300 pulses at 10 Hz was tried. Sensitive power-in-the bucket of a HeNe reference beam has verified this conclusion. I am unaware of any [other] holographic gratings with high damage thresholds."

4. The gratings appear to be as durable as the substrate material itself.

Quality of the Etch

One way to quickly measure the quality of a diffraction grating is to measure its maximum diffraction efficiency,

η_{max}, where the efficiency, η, is given by Eq. 20. As in previous chapters, measurements were made using the geometry of Fig. 4 with a right angle prism substituted for the wedge prism.

Figures 26 and 27 show the maximum grating efficiency, η_{max}, as a function of etch depth for free space wavelengths of 457.9 nm and 632.8 nm, respectively. The numbers labeling each data point correspond to the substrate identification numbers as listed in Table IV. For most gratings, the etch depth was determined from SEM photographs. However, the depths of gratings 4, 5, 7 and 11 were calculated using measured birefringence data--see Chapter VI. In Fig. 26 and in those following, circular data points are used when grating depth was measured from SEM photographs while square data points indicate that grating depth was calculated.

Figures 26 and 27 both illustrate the strong correspondence between etch depth and efficiency which is characteristic of high-frequency holographic diffraction gratings. Note that in the best case (grating 5) maximum diffraction efficiency exceeds 85%. Thus, the quartz replicas are as good as the photoresist originals (compare with data from Fig. 21).

Another way to measure etch quality is to inspect the gratings with the aid of an SEM. Figures 28 and 29 contain SEM photographs of two of the etched gratings. Compare

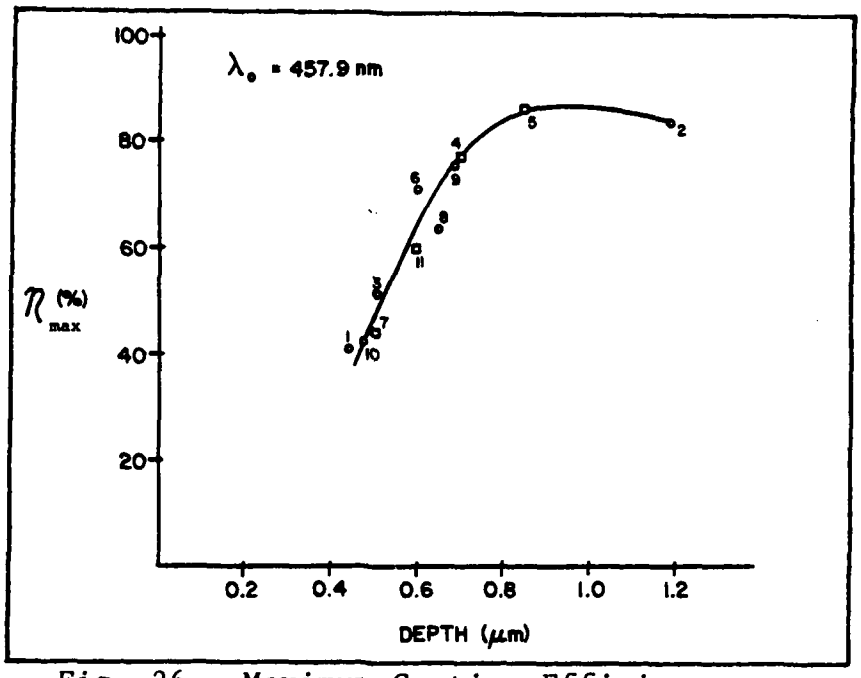

Fig. 26. Maximum Grating Efficiency vs. Etch Depth--Quartz Gratings

Key: Numbers Identify Gratings--see Table IV
Circle = Depth Measured from SEM Photo
Square = Depth Calculated from Birefringence Data--see Chapter VI

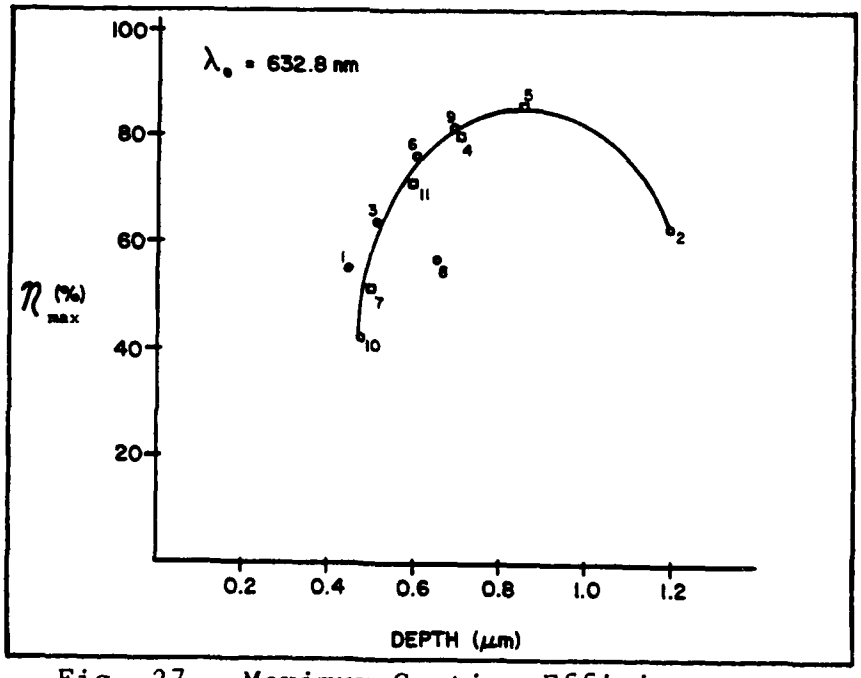

Fig. 27. Maximum Grating Efficiency vs. Etch Depth--Quartz Gratings

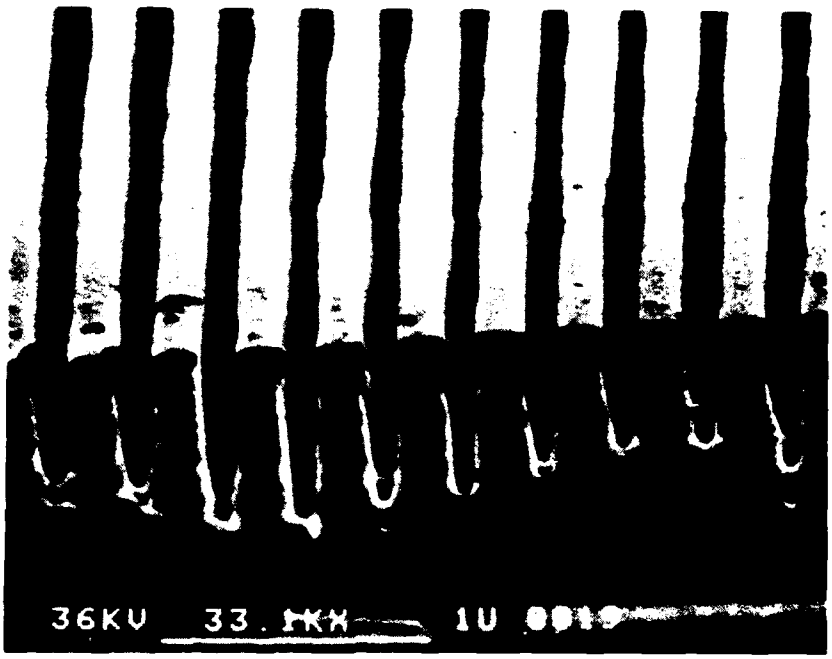

Fig. 28. SEM Photograph of Quartz Grating #1
Scale: Horizontal Line at Bottom of Photo Equals 1 μm

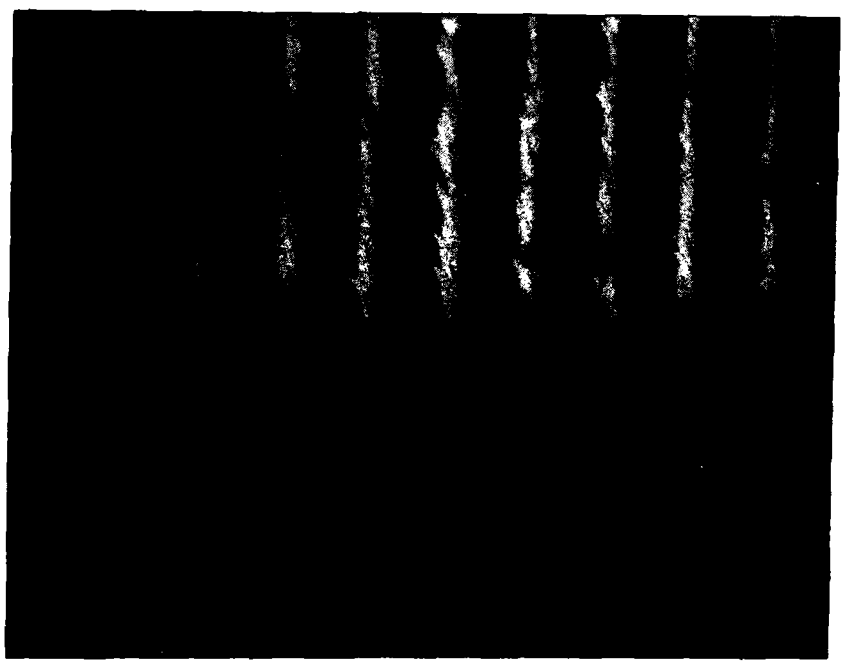

Fig. 29. SEM Photograph of Quartz Grating #8
Scale: Horizontal Line at Bottom of Photo Equals 1 μm

these photographs with those in Fig. 25 which are SEM photographs of a photoresist grating similar to the ones prepared as etching masks for the quartz gratings. Note that the grating in Fig. 28 is different from the rest in that the fringes have flat tops. This is caused by insufficient etching time. On the other hand, the grating fringes in Fig. 29 look very much like the photoresist mask fringes. This explains why our best quartz gratings have efficiencies comparable to the photoresist gratings. Reactive ion etching faithfully transferred the photoresist pattern into the quartz. The quality of the etch is excellent.

Grating Replication

In this final section of Chapter V we briefly report on another fabrication technique which also produces more durable gratings than those made in photoresist. This fabrication method is actually a replication technique and so holds promise as an inexpensive way of producing production quantities of gratings.

A photoresist master was made using the procedures described in Chapter III. Prior to chrome coating, the photoresist grating had a maximum diffraction efficiency, η, of approximately 82% under 632.8 nm illumination. The master was then coated with between 0.2 μm and 0.3 μm of chrome, to increase the rigidity of the master. To replicate the grating, the master was then coated with a mixture of UV curable

HHA/HDDA polymer. Both HHA and HDDA are 3M products. The HHA is thick when uncured and abrasion resistant when cured. The HDDA acts as a thinner for the HHA so that the HHA/HDDA mixture fills in between the grating fringes. The chrome coating and HHA/HDDA processing were done by Don Kerfeld at 3M[45].

After curing, the master hologram was separated from the polymer copy. Testing revealed that the cured replica had a 54% maximum diffraction efficiency at 632.8 nm. In addition, although the replica could be scratched, it was much more durable than the original photoresist master. Touching the replica appeared, initially, to destroy it. However, with time the grating reappeared, suggesting that finger moisture acted as an index matching fluid temporarily destroying the diffractive properties of the grating replica.

Our more recent research suggests that the poorer diffraction efficiency of the curved replica was probably due to insufficient groove depth, perhaps caused by inadequate penetration of the HHA/HDDA polymer in between the master photoresist grooves. A different mixture ratio might solve the problem. We did not pursue this problem further for two reasons: first, because reactive ion etching proved so successful; and secondly because we had achieved our objective of proving that durable replicas can be made of holographically recorded patterns with extremely fine periodic

features (i.e. periods less than 0.35 μm). The polymer copies, because of their potential low cost, should be further investigated by persons interested in high volume commercial applications.

VI. Optical Elements Formed via Ultra-High Spatial-Frequency Surface Corrugations

In this chapter we discuss two new applications of the quartz gratings described in Chapter V. We have discovered that optical surfaces containing deep grooves have broadband antireflective properties rivaling the best antireflection (AR) coatings. Also, in transmission these optical elements exhibit artificially produced birefringence which makes them suitable candidates for use as waveplates. These findings, especially when coupled with the damage resistance of our quartz gratings (reported in Chapter V), are particularly significant because the size of the grooves can be scaled for use in the UV and IR where damage resistant AR coatings and transparent birefringent materials may not exist.

Antireflection Coatings

Antireflection coatings are used in a wide variety of applications from non-glare glass to the windows and other optical surfaces in many lasers. When used on optical elements, such as with lasers, there are three requirements AR coatings must satisfy. First, they must have low reflectance (usually less than 0.1%) to reduce backreflection and thus prevent damage to sensitive elements from the high power inside a laser cavity. Secondly, to enhance the transmittance of the laser, AR coatings must have low absorption and minimal scattering characteristics. Thirdly,

AR coatings must have a high damage threshold to withstand laser radiation, especially when used with high power lasers[46]. It is this third requirement that Crane[44] claims our quartz gratings satisfy better than gratings now commercially available (see Chapter V).

There are many types of AR coatings in use today. The most simple AR coating is a single layer of film. In theory, when the optical film thickness is equal to one-quarter of the wavelength of the incident radiation and the film's index of refraction is equal to the square root of the substrate's refractive index, then the reflectance in air is zero. In practice, this type of coating is rarely used since a material with the required index of refraction is usually hard to find[47]. For example, there is no inorganic material available for use in air with commercial soda-lime glass, the material we used as a substrate for our photoresist gratings. The lowest index inorganic material widely used in industry today has an index of 1.38 (vs. the 1.23 needed)[48]. This is especially significant since, as we report in this chapter, our photoresist gratings act as a single layer AR coating for soda-lime glass.

A very popular AR coating is the V-coating. V-coatings are two-layer coatings which theoretically have a zero reflectance at just one wavelength. The name comes from the shape of the power reflectance curve as a function of wavelength[49]. Ideally, the coating contains two layers,

each one-quarter wavelength thick. However, as with single layer coatings, it is often difficult to find appropriate materials. Thus, in practice, layers of varying thickness are used. Typically, the refractive index of the inner layer is higher than the substrate index, while the outer layer has a lower index of refraction[46].

The above discussion has addressed AR coatings for single wavelength applications only. However, broadband AR coatings are also available. Typically, such coatings consist of multiple layers of varying thickness and index[50]. Thus, in general, a designer of AR coatings has a variety of parameters to work with: the number of layers; the thickness, refractive index, and absorption coefficient of each layer; and finally in some applications even the choice of substrate and surrounding medium[51].

Aside from the difficulty of designing and then finding suitable materials for AR coatings, there are other problems as well. In production, difficulties arise in the control of layer thickness and refractive index[49]. In use, touching an AR coating often destroys it, especially in high power applications[52].

In this chapter we suggest an alternative to dielectric coatings. Our diffraction gratings, whether in a single layer of photoresist or etched in quartz substrates, have very low broadband reflectivities. In addition, our quartz gratings, if accidentally touched, can be cleaned and reused.

Antireflection Properties of our Quartz Gratings

In the course of our study of high-frequency holographic diffraction gratings we discovered that at normal incidence these gratings have very low reflectivity. Figures 30 and 31 are graphs of grating reflectivity (in percent) for near normal illumination at 457.9 nm and 632.8 nm, respectively. In all cases, the light polarization was perpendicular to the grating fringes. Data were collected using the configuration shown in Fig. 32 where reflectivity equals I_{R2}/I_{IN}. Note that in the best case, the reflectivity is reduced by a factor of 87 from the standard 3.5% reflectivity of fused quartz (index of refraction of 1.46[53])[§]. This low reflectivity is particularly important when one considers that no optical coatings of any kind are present on the grating surface. The gratings can be washed in solvents such as acetone without any loss of efficiency or antireflectivity. Thus, these gratings appear to represent a durable alternative to multilayer dielectric coatings.

One of the questions raised during our research was whether the gratings are in fact antireflectors, or whether

---

[§]Actually, as we show in a subsequent figure in this chapter, our best quartz grating has a reflectivity of 0.035%. This is 100 times lower than the reflectivity expected from flat fused quartz. In Figs. 30 and 31, reflectivities have been rounded to the nearest hundredth of a percent for graphing.

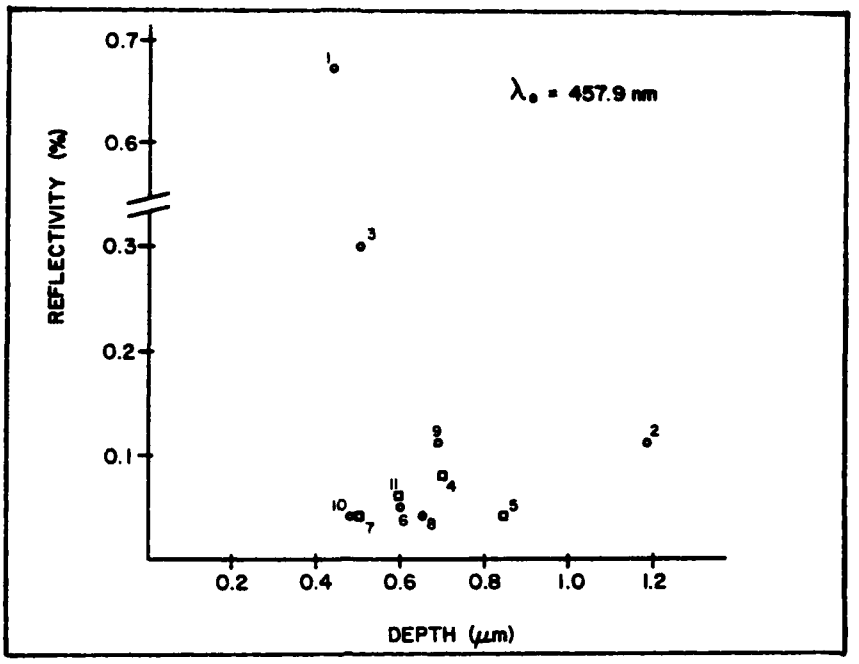

Fig. 30. Grating Reflectivity In Percent (At Normal Incidence) vs. Etch Depth--Quartz Gratings

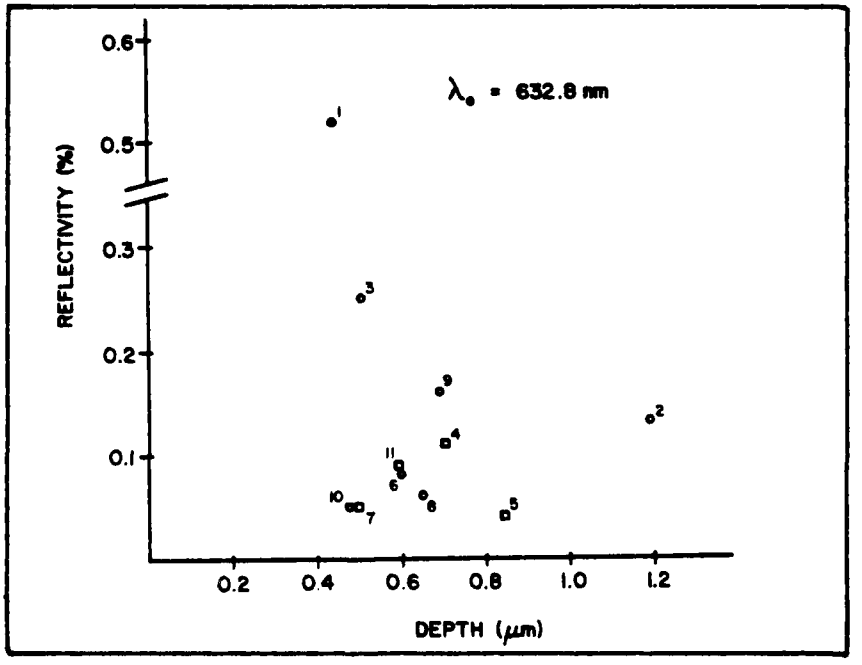

Fig. 31. Grating Reflectivity In Percent (At Normal Incidence) vs. Etch Depth--Quartz Gratings

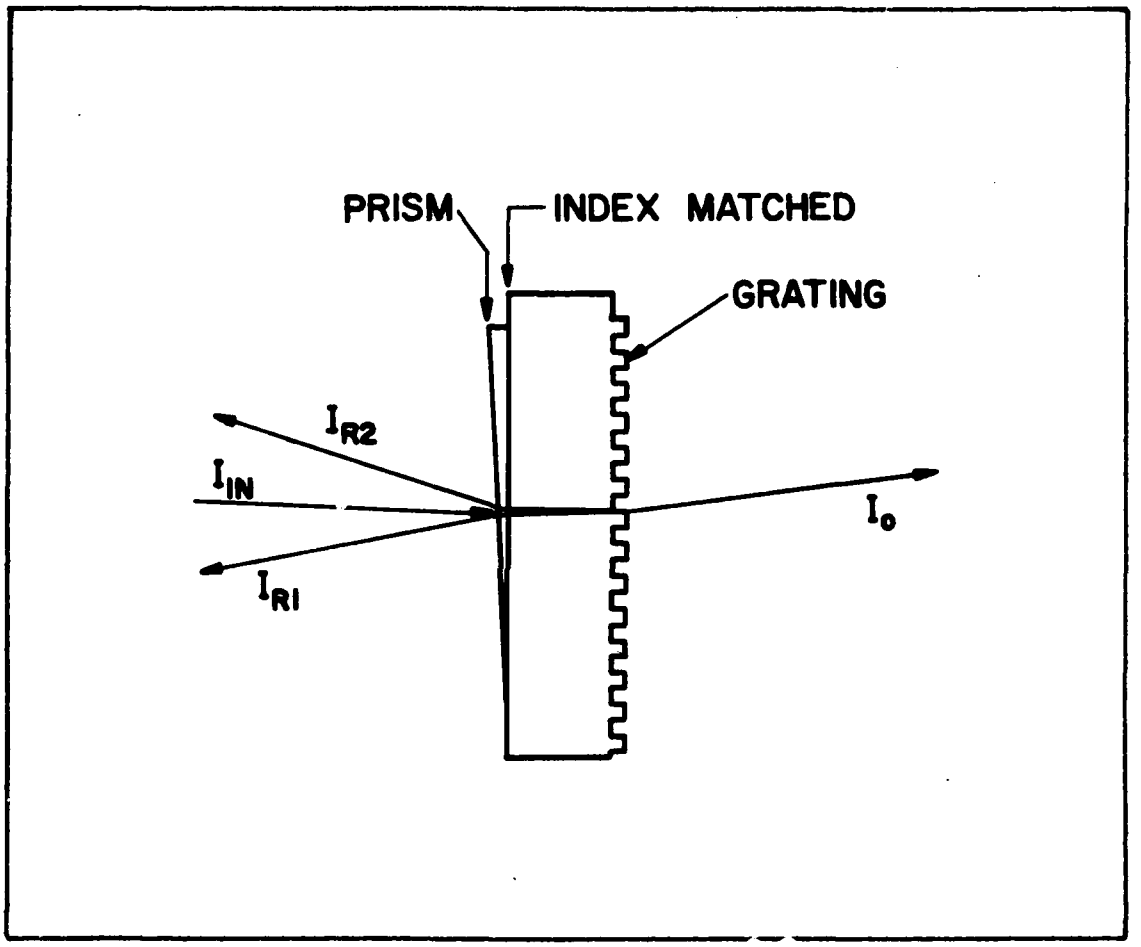

Fig. 32. Geometry Used to Measure Reflectivity From Quartz Gratings at Near Normal Incidence

AD-A132 355 HOLOGRAPHIC OPTICAL ELEMENTS WITH ULTRA-HIGH SPATIAL FREQUENCIES(U) AIR FORCE INST OF TECH WRIGHT-PATTERSON AFB OH R C ENGER 1983 AFIT/CI/NR-83-35D 2/2

UNCLASSIFIED F/G 20/6 NL

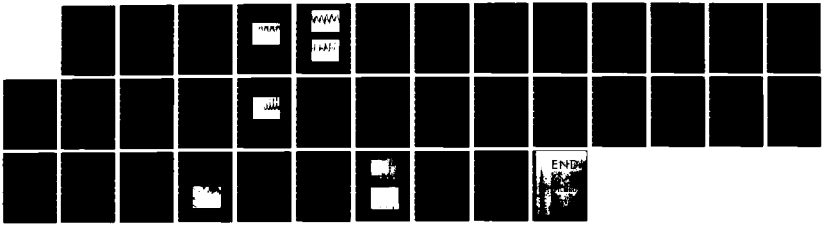

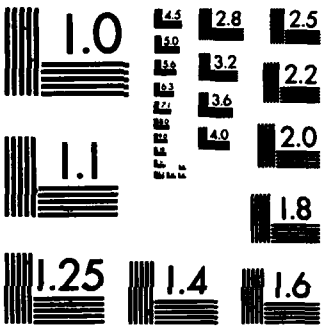

MICROCOPY RESOLUTION TEST CHART
NATIONAL BUREAU OF STANDARDS-1963-A

the corrugated grating surfaces are just acting like ground glass, scattering the light in all directions. If our gratings are equivalent to AR coatings, then light that is not specularly reflected will be transmitted and not scattered.

To test the transmission characteristics of our gratings we used 632.8 nm light perpendicularly polarized to the grating fringes. Since, under normal (0°) illumination, the expected reflection from a flat quartz substrate is 3.5% per side, such a substrate will transmit approximately 93.1% of the light it receives at normal incidence. However, if one side is perfectly AR coated, then the maximum theoretical transmission is 96.5%.

Our best grating, grating 5, which has a grating on one side and is flat on the other, has a measured transmission, at normal incidence, of 97 ± .5%. When the backs of gratings 5 and 10 are placed back-to-back and are index matched together with xylene, the measured transmission, at normal incidence, is 99.5 ± .5%. These measurements prove that the gratings are in fact acting as antireflectors, transmitting the light which is not specularly reflected.

Because of the difficulty in distinguishing one grating from another in transmission, we have chosen to report our findings in terms of specular reflectivity rather than in terms of transmissibility.

Unlike Figs. 26 and 27, Figs. 30 and 31 illustrate that there is no identifiable relationship between depth and

reflectivity. Rather, our results indicate that the shape of the grating profile is the dominant factor governing reflectivity. We speculate that low reflectivity results because the grating surface profile appears to the incoming light wave to be a surface whose average index of refraction is smoothly tapered from that of air to that of the grating substrate. To support this speculation we present Figs. 33, 34, and 35.

Figures 33, 34, and 35 are SEM pictures of three different gratings, all having roughly the same depth but different reflectivities. Figure 35 is a picture of one of the gratings with the lowest reflectivity, grating 8, while Fig. 33 is a picture of one of the gratings with the highest reflectivity, grating 3. In comparing these two photographs, note that lower reflectivity results when the grating fringe profile varies smoothly. For example, in Fig. 35 the grating fringes are nearly triangular in shape.

We can speculate as follows as to why the subwavelength fringe shape affects reflectivity. Suppose this grating is divided into a series of slices, each parallel to the surface of the grating substrate. Considering slices in order from top to bottom in Fig. 35, the average index of refraction of each slice will always be slightly higher than the average index of the slice above it. Thus, as a light wave penetrates the grating it will gradually encounter material with larger and larger average indices of refraction. In

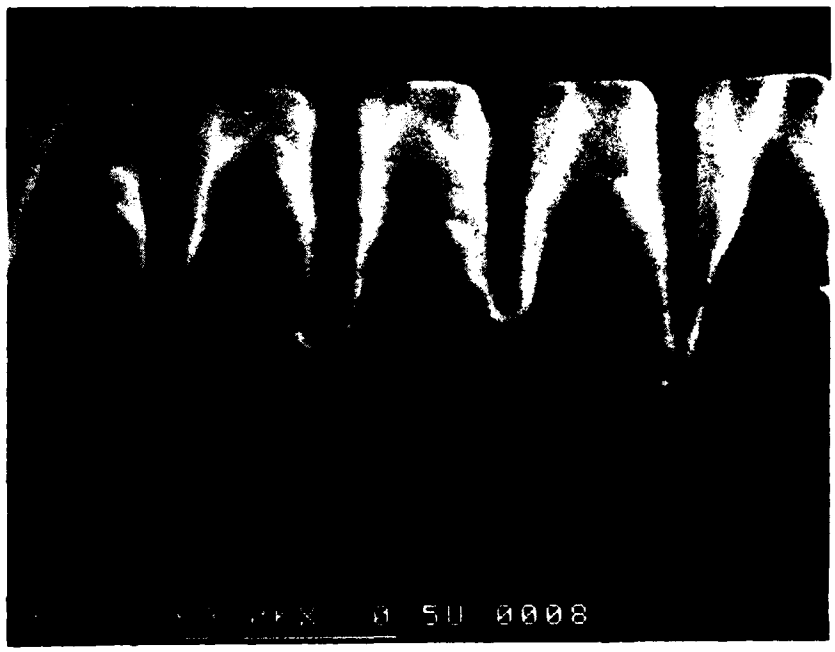

Fig. 33. SEM Photograph of Grating #3 Showing Grating Profile Horizontal Line Equals 0.5 μm

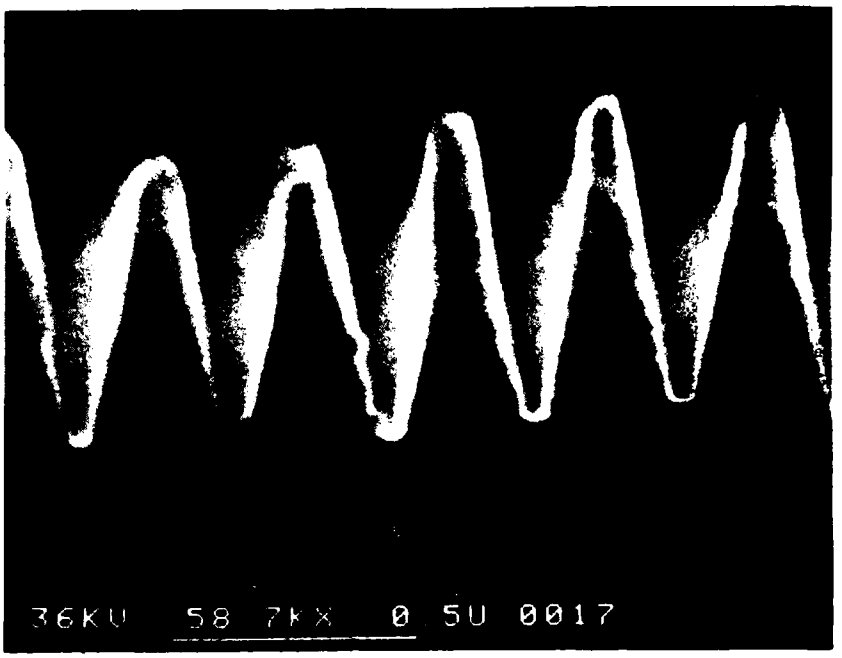

Fig. 34. SEM Photograph of Grating #9 Showing Grating Profile Horizontal Line Equals 0.5 μm

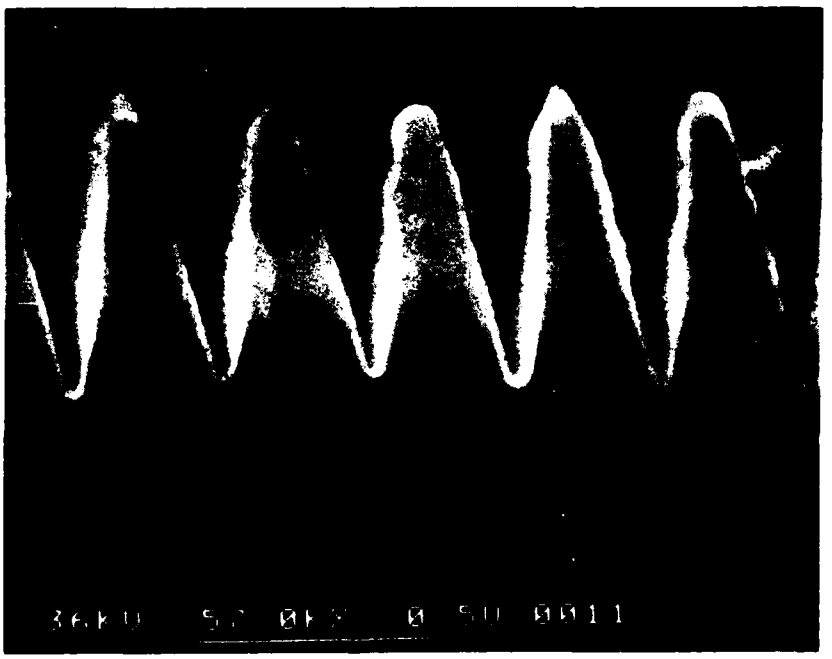

Fig. 35. SEM Photograph of Grating #8 Showing Grating Profile Horizontal Line Equals 0.5 μm

contrast, the grating fringes in Fig. 33 are flat on top, as if the triangular peaks have been cut off. This structure is caused by insufficient etching time. The top slice of this grating profile has an average index much greater than that of air. Thus, when a light wave encounters the top of this grating it sees a significant index discontinuity.

Consistent with our argument above, the reflectivity of grating 9, shown in Fig. 34, is much lower than the reflectivity of grating 3 (Fig. 33) but slightly higher than the reflectivity of grating 8 (Fig. 35). Note that the bottom of the grooves of grating 9 are slightly rounded and broader than those of grating 8. In geometric terms, grating 9 is more sinusoidal while grating 8 is more triangular in shape. Thus, for lowest reflectivity, a grating should have triangularly shaped fringes.

The observations made above regarding Figs. 33, 34, and 35 are in agreement with theoretical predictions (albeit for a different readout geometry) in the work of Moharam and Gaylord[3]. Although Moharam and Gaylord were not considering the case of a non-diffractive readout geometry, we note in their Figs. 4 and 6 that the amplitude of the specular reflection tapers monotonically toward zero when the grating has a smoothly tapered fringe profile (i.e. sinusoidal or triangular grating). For a triangular grating profile the specular reflection component reaches zero when the grating depth-to-period ratio reaches 0.6. Interestingly though,

the specular reflection for the sinusoidal grating never reaches zero. It levels off at nearly zero when the depth-to-period ratio is approximately 0.6. This finding is essentially in agreement with our experimental results; our triangularly shaped grating has the lowest reflectivity and a depth-to-period ratio greater than 0.6.

Moharam and Gaylord's Fig. 5 is an analysis of a square-wave-type grating. Here the surface profile has abrupt discontinuities and thus abrupt changes in the average index of refraction. In some respects, our grating 3 shown in our Fig. 33 has a square-wave profile. Consistent with our comments above, the square-wave grating analyzed by Moharam and Gaylord[3] has a periodic specular reflection which never goes to zero but which instead oscillates as the depth-to-period ratio changes. This oscillation is similar to the specular reflection expected from a dielectric coating whose thickness is monotonically increased.

Perhaps the most appealing feature of our gratings, as antireflectors, is that they are very broadband; that is, they have low reflectivity throughout the visible spectrum. For example, Fig. 36 is a graph showing the specular reflectivity of grating 5 as a function of normally incident illumination throughout the visible spectrum. Note that even in the worst case the grating reflectivity is less than 0.045%, a reflectivity more than 75 times lower than that of fused quartz.

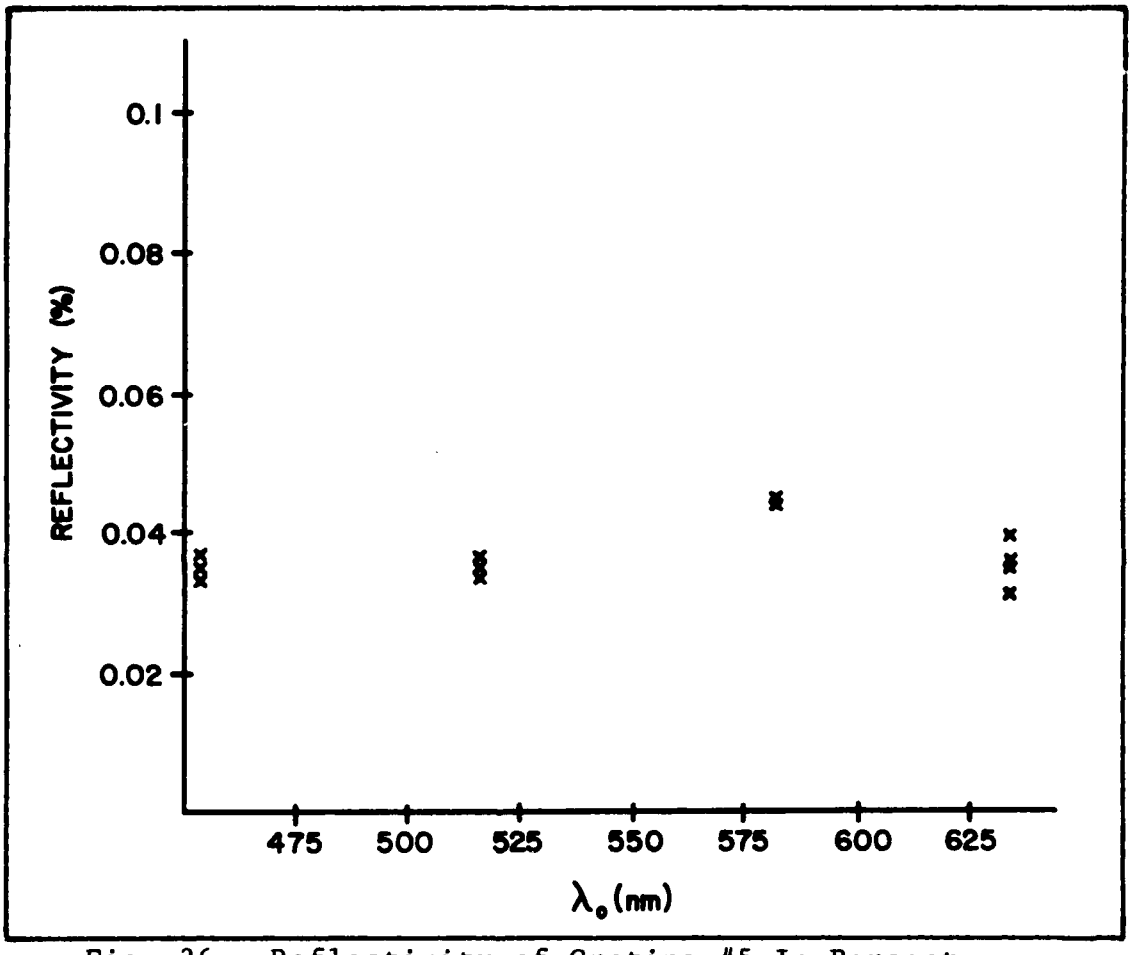

Fig. 36. Reflectivity of Grating #5 In Percent
vs. Wavelength
(Measured At Normal Incidence)
X's Indicate Each of Several Measurements

Antireflection Properties of our Photoresist Gratings

Just as with our quartz gratings, we have found that the high-frequency photoresist gratings described in Chapter V also have antireflective properties. In some respects, this feature is analogous to the use of porous oxides as AR coatings[48]. Since the index of refraction of a material is related to its density, single layer AR coatings for glass can be made by artificially reducing the index of refraction of certain materials, such as aluminum oxide, by introducing porosity. In a recent study by Yoldas, reflectivity of porous oxide-coated glass was reduced to 1.4% at approximately 600 nm.

Unlike our gratings, the pore size used by Yoldas is substantially smaller than the wavelength of light (on the order of 80 Å in diameter) and the distribution is homogeneous[48]. However, just as we suggested when discussing the quartz gratings in the previous section, the key parameter is a change in the index of refraction of the boundary layer.

We have not attempted to optimize antireflectivity with our photoresist gratings. However, in limited tests of existing samples the lowest reflectivity (at normal incidence) we have obtained to date is 0.5% at 632.8 nm. The substrate, soda-lime-glass, has a theoretical reflectivity of 4.1% (index of refraction is 1.51). Thus, a photoresist

grating is essentially a single layer AR coating for soda-lime glass.

Our decision not to pursue thorough testing of the photoresist gratings as AR coatings is based on the vulnerability of photoresist gratings to damage as discussed in previous chapters. Photoresist gratings suffer from essentially the same limitations as conventional AR coatings.

Gratings as Waveplates

Quarter waveplates are used today in numerous applications. Typically, they are made from materials which are N + 1/4 wavelengths thick where N is some integer. One of the difficulties with these waveplates is that when used with slightly different wavelengths, their performance degrades rapidly. Yet there are important multiple wavelength applications. For example, in videodisk technology different diode lasers are used for read and write[54].

One way to minimize the degradation of waveplate performance with changing wavelength, is to make first order waveplates where N = 0. Unfortunately, to satisfy this criterion with conventional waveplates, either a very thin waveplate or two waveplates with opposing fast and slow axis' must be used, making the element difficult to fabricate and expensive.

We believe a solution to this problem can be found by adapting millimeter-wave technology to the visible spectral

domain. In millimeter-wave antenna applications, metallic gratings known as "corrugated-surface twist polarizers" are used to rotate the polarization of incident waves. Such devices, used in reflection, are found in scanned reflector antenna systems and on the main and subdishes of microwave Cassegrain antennas[55,56].

Although used in transmission rather than reflection, our corrugated surface optical elements have surface features similar to those of twist polarizers. Furthermore, upon detailed study of both our photoresist masks and quartz replicas, we discovered that they also have birefringent properties similar to those of twist polarizers. In this section we discuss this phenomenon and offer a method of evaluating the performance of such optics.

Consider the optical arrangement shown in Fig. 37. Assume a plane wave emerges from the first linear polarizer oriented at 45° with respect to the horizontal so that

$$\vec{E}_{IN} = E_x e^{j(\omega t + \phi)} [\hat{x} + \hat{y}] \tag{21}$$

Suppose this wave impinges on a transparent birefringent material with fast and slow axis' in the $\hat{x}$ and $\hat{y}$ directions. The emerging wave would be

$$\vec{E}_t = E_x e^{j(\omega t + \phi + kDn_x)} [\hat{x} + e^{j(\Delta\phi_n)} \hat{y}] \tag{22}$$

where

$$\Delta\phi_n = \frac{2\pi D}{\lambda_o} (n_y - n_x) \tag{23}$$

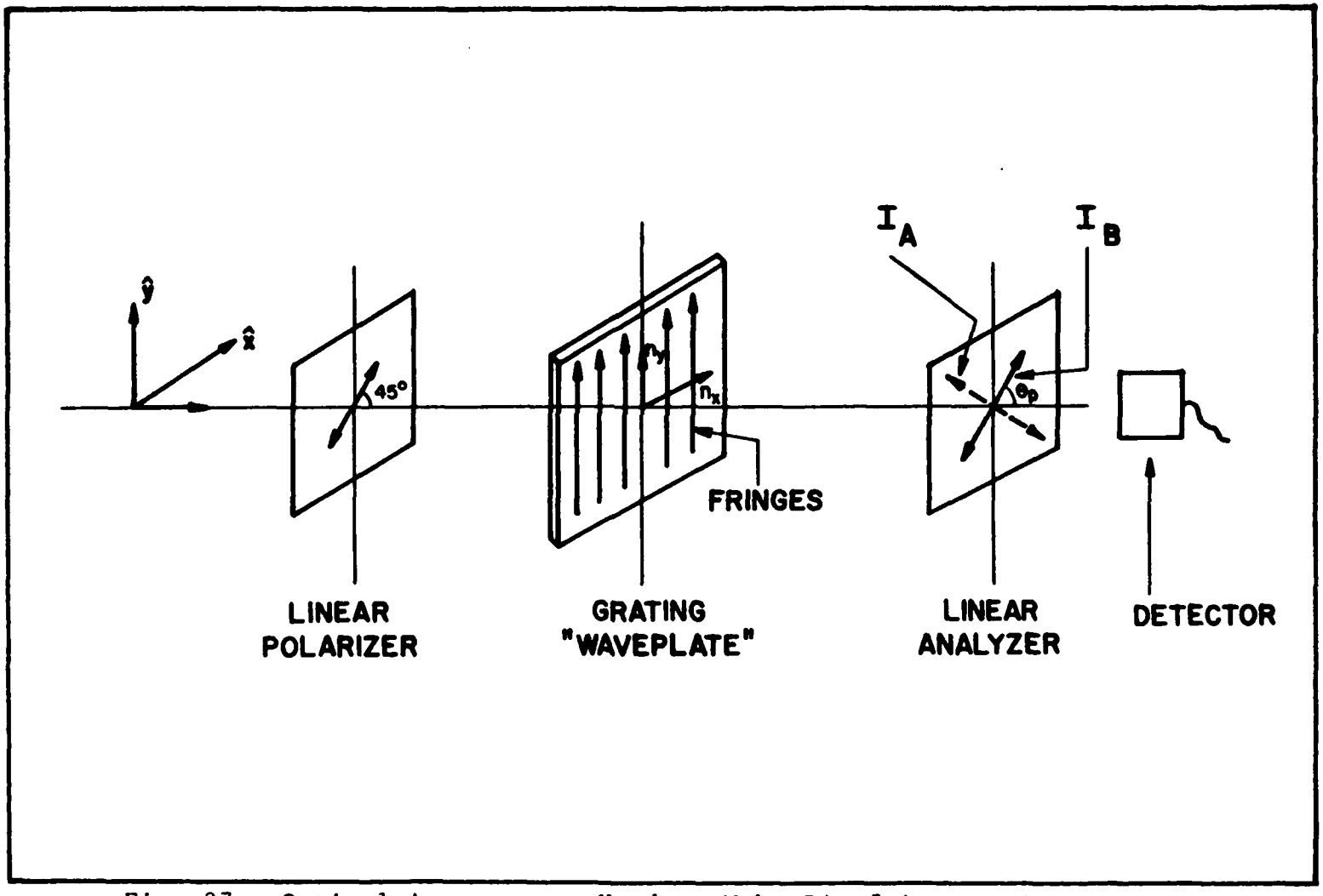

Fig. 37. Optical Arrangement Used to Make Birefringence Measurements

Here n_x and n_y are the indices of refraction for light polarized in the $\hat{x}$ and $\hat{y}$ directions, respectively. Furthermore, since the transmittance of a linear polarizer is

$$\vec{T}_p = \cos\theta_p \hat{x} + \sin\theta_p \hat{y} \tag{24}$$

where θ is measured from the horizontal, the wave emerging from the linear analyzer is

$$\left|\vec{E}_{out}\right| = \vec{E}_t \cdot \vec{T}_p$$
$$= E_x e^{j(\omega t + \phi + kDn_x)} [\cos\theta_p + e^{j(\Delta\phi_n)} \sin\theta_p] \tag{25}$$

Thus, a detector placed to the right of the analyzer in Fig. 37 would measure

$$I_{out} = \vec{E}_{out} \cdot \vec{E}^*_{out} = E_x^2[1 + 2\cos\theta_p \sin\theta_p \cos(\Delta\phi_n)] \tag{26}$$

In our case the birefringent material is one of our gratings. To measure the birefringence of our gratings, we oriented the fringes along the $\hat{y}$ direction as shown in Fig. 37. We then measured the transmitted intensity (through the analyzer) when the analyzer was oriented at -45° and 45°, giving us (using Eq. 26)

$$I_A = \frac{|E_{IN}|^2}{2}[1 - \cos(\Delta\phi_n)] \tag{27}$$

and

$$I_B = \frac{|E_{IN}|^2}{2}[1 + \cos(\Delta\phi_n)] \tag{28}$$

Dividing Eq. 27 by Eq. 28 and solving for the effective phase change due to the grating, $\Delta\phi_n$, gives

$$\Delta\phi_n = \cos^{-1}\left[\frac{1 - R}{1 + R}\right] \tag{29}$$

where

$$R = \frac{I_A}{I_B} \tag{30}$$

When $\Delta\phi_n = \pi/2$, the grating is a quarter waveplate. Thus, the birefringent performance of a corrugated surface optical element can be evaluated by measuring I_A and I_B and then calculating $\Delta\phi_n$. Table VIII contains a listing of $\Delta\phi_n$ for each of our quartz gratings, measured at 457.9 nm and 632.8 nm.

Note from Table VIII that $\Delta\phi_n < \pi/2$ for all of the quartz gratings. Thus, none of our quartz gratings is in fact a quarter waveplate. However, by combining two or more gratings in tandem, quarter waveplates can be obtained. We verified this experimentally with several combinations and were able to produce quarter waveplates with $\Delta\phi_n$ within 1% of $\pi/2$.

Using Eq. 23 and the known depths of the grating grooves from our SEM pictures, we calculate the magnitude of the difference in index of refraction, $|n_y - n_x|$, for our gratings as 0.06. Thus, again using Eq. 23, for a grating to be a quarter waveplate it must have a depth of 2.0 μm under 457.9 nm illumination and a depth of 2.7 μm at

Table VIII
Effective Phase Change, $\Delta\phi_n$, Due to the Grating

Grating #	$\Delta\phi_n$ (radians) (at 457.9 nm)	$\Delta\phi_n$ (radians) (at 632.8 nm)
1	0.40	0.30
2	0.90	0.62
3	0.41	0.31
4	0.55	0.41
5	0.66	0.49
6	0.54	0.41
7	0.37	0.29
8	0.52	0.39
9	0.54	0.39
10	0.36	0.28
11	0.47	0.34

632.8 nm. Figures 38 and 39 illustrate the relationship between phase shift and depth at these two wavelengths.

It should be noted that results similar to those described above were obtained when we used the photoresist masks instead of the quartz gratings. Also, although crystalline quartz has some birefringence, the fused quartz substrates we used, by themselves, had no measurable birefringence and thus did not contribute to our results.

Our experiments verify that groove depth is the critical parameter when making grating quarter waveplates. With the mask and reactive ion etching technology we employed we

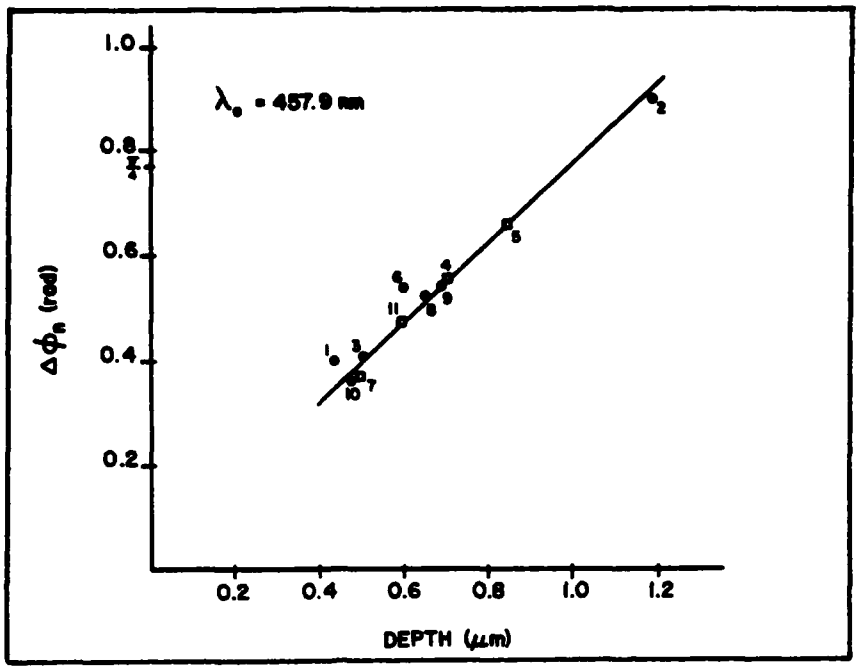

Fig. 38. Effective Phase Shift vs. Etch Depth--Quartz Gratings

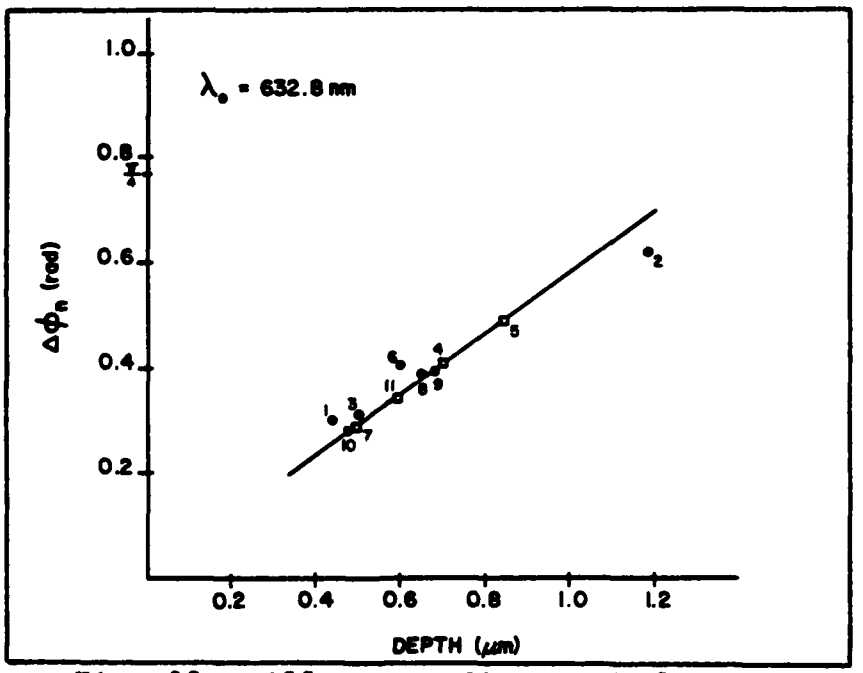

Fig. 39. Effective Phase Shift vs. Etch Depth--Quartz Gratings

were unable to obtain groove depths greater than 1.2 μm. Figure 40 is a SEM photograph of our most deeply etched substrate showing the groove depth of nearly 1.2 μm. Because a single element quarter waveplate requires still deeper groove depths, we suggest consideration of 2-layer masking technology[57,58] as a way to increase etch depth.

The fact that high-frequency holographic diffraction gratings are birefringent is an important discovery. The gratings, in quartz, are very durable, can be cleaned with solvents such as acetone or methanol, and when stacked act as first order waveplates in the visible spectrum. Our findings are especially significant in that by using this technique, waveplates can potentially be made from any material for use at any wavelength. This may be especially important in the UV or IR where suitably transparent and birefringent natural materials may not exist.

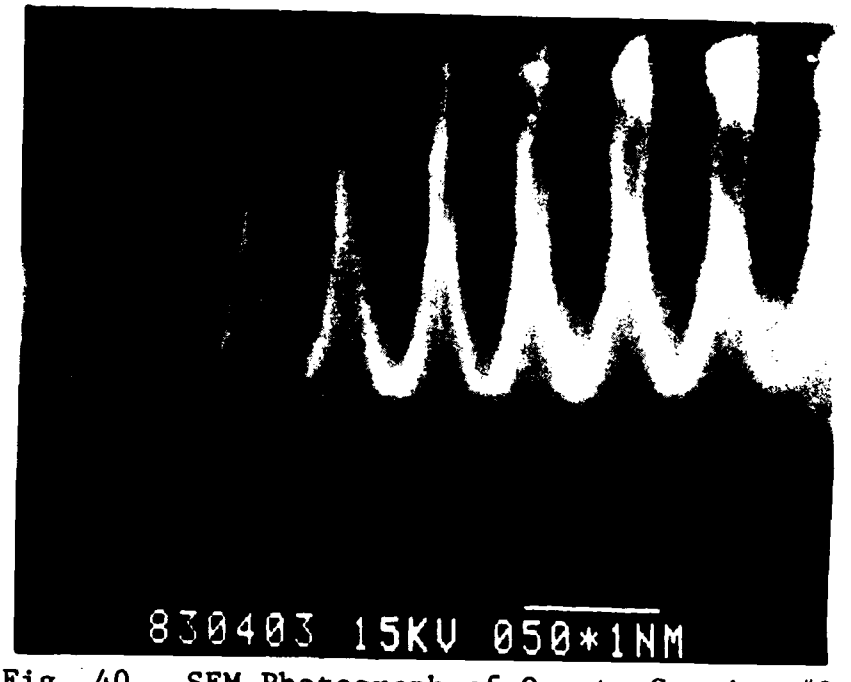

Fig. 40. SEM Photograph of Quartz Grating #2
Scale: Horizontal Line at Bottom of
Photo Equals 0.5 m

VII. Summary and Conclusions

The objectives and original contributions of this dissertation can be grouped into four categories: production and thorough analysis of high-frequency diffraction gratings in photoresist with efficiencies significantly higher than previously obtained and approaching the theoretical limit; extension of the proven resolution limits of Shipley AZ-1350 series photoresist; development of a process to greatly improve the durability of surface relief optics without sacrificing desirable optical qualities; and discovery and study of two new properties of our holographic optical elements (HOEs).

Our research demonstrates that holographic diffraction gratings can be produced in photoresist with transmission diffraction efficiencies (greater than 88% at 632.8 nm) rivaling those made in dichromated gelatin and other volume holographic materials. However, unlike dichromated gelatin, our photoresist gratings have the desirable surface-relief features needed for potentially inexpensive replication.

As a result of our efforts to produce high-efficiency diffraction gratings in photoresist, we have extended the proven resolution limits of Shipley AZ-1300 series positive photoresist by a factor of 2 from 1500 ℓ/mm to over 3000 ℓ/mm. We demonstrate in this thesis, as evidenced by the SEM photographs, that depth to period ratios exceeding 1.1 can be achieved even when spatial frequencies are as

high as 3000 ℓ/mm. Furthermore, these large feature sizes can be produced using standard holographic techniques without the use of pre or post exposures or ion milling.

Our thorough study of high-frequency photoresist gratings has resulted in several important findings. First, although the efficiency of our high frequency photoresist gratings is relatively high throughout the visible spectrum, both efficiency and angular selectivity increase with wavelength. Secondly, there is an enhancement in diffraction efficiency if the reconstruction beam is incident near the critical angle of the holographic substrate. Thirdly, and most importantly, this enhancement is considerable when the theoretical Bragg angle is near the critical angle.

In addition to learning more about the transmission diffraction efficiency of photoresist gratings, we have also discovered that the gratings act as strong specular reflectors at certain angles of reconstruction beam incidence, θ. The most pronounced reflection occurs just prior to emergence of the diffracted order.

Many of our gratings are now over a year old. We have noticed no measurable decrease in diffraction efficiency with time. However, photoresist gratings are rather delicate and should only be used in applications where they can be protected from accidental contact with foreign objects.

To extend the usefulness of the surface relief gratings made in photoresist we have successfully developed a

procedure, using reactive ion etching technology, which faithfully transfers the photoresist pattern to fused quartz. Just as with the photoresist gratings, our best quartz grating has a diffraction efficiency greater than 85%.

Reactive ion etching also greatly improves the durability of surface relief optics without sacrificing desirable optical qualities. Our tests of the optical elements etched in quartz indicate that these elements are as durable as the substrate material itself. The best grating tested withstood fluxes as high as 4.17 GW/cm^2 without sustaining damage. Surprisingly, even as many as 300 pulses at a 10 Hz repetition rate failed to degrade grating 3 even though multiple pulses are usually more damaging to materials than a single pulse. As further evidence of durability, we note that dirt and grease can be safely removed with solvents such as acetone or methanol. Although the quartz gratings can be scratched, they are much more scratch resistant than the photoresist gratings.

The high frequency of our photoresist and quartz gratings guarantees that all diffracted orders are evanescent under normal incidence illumination. This property has led to the discovery of two new applications for high-frequency holographic diffraction gratings; that is, these gratings can be used as AR coatings and as waveplates.

Our optical elements, especially the quartz gratings, have extremely low reflectivity and consequent high transmittance at normal incidence. In fact, our best element has a reflectivity which is 100 times less than that theoretically expected from planar fused quartz. Furthermore, these are broadband antireflectors. Over the entire visible spectrum they satisfy the requirement for good AR coatings that reflectivity be less than 0.1%. In conventional AR coating technology only complex multilayer dielectric coatings approach these performance characteristics; and even these multilayer coatings are inferior when durability comparisons are included. In fact, it is primarily the durability of these elements that makes them exciting alternatives to multilayer dielectric coatings.

In addition to durability, the thickness of the gratings and their surface-relief features have led to a second new application. Our gratings exhibit artificially produced birefringence. When etched to the proper depth, these gratings can act as first order waveplates.

The antireflective and birefringent natures of our photoresist and quartz gratings may be particularly significant in the UV and IR where damage resistant AR coatings and transparent birefringent materials may not exist.

Bibliography

1. D. H. McMahon, A. R. Franklin, and J. B. Thaxter, Appl. Opt. 8, 399 (1969).

2. C. J. Kramer, SPIE Proc. Symp. on High Speed Read/Write Techniques for Advanced Printing and Data Handling 390 (to be published).

3. M. G. Moharam and T. K. Gaylord, J. Opt. Soc. Am. 72, 1385 (1982); erratum 73, 411 (1983).

4. D. H. Close, Opt. Eng. 14, 408 (1975).

5. N. K. Sheridon, Appl. Phys. Lett. 12, 316 (1968).

6. D. Rudolph and G. Schmahl, Optik 30, 475 (1970).

7. R. Bartolini, W. Hannan, D. Karlsons, and M. Lurie, Appl. Opt. 9, 2283 (1970).

8. M. J. Beesley and J. G. Castledine, Appl. Opt. 9, 2720 (1970).

9. R. A. Bartolini, Appl. Opt. 13, 129 (1974).

10. F. Iwata and J. Tsujiuchi, Appl. Opt. 13, 1327 (1974).

11. R. Kurtz and R. Owen, Opt. Eng. 14, 393 (1975).

12. R. C. Enger and S. K. Case, "High-Frequency Holographic Transmission Gratings in Photoresist", to be published in J. Opt. Soc. Am.

13. S. L. Norman and M. P. Singh, Appl. Opt. 14, 818 (1975).

14. S. Austin and F. T. Stone, Appl. Opt. 15, 1071 (1976).

15. R. F. Stevens and M. C. Hutley, SPIE Proc. Advances in Optical Production Technology 163, 84 (1979).

16. R. A. Bartolini, H. M. Smith (editor), Topics In Applied Physics, Vol 20, Springer-Verlag, New York (1977).

17. W. T. Tsang and S. Wang, Wave Elec. 1, 85 (1974/75).

18. Shipley, Technical Data, 1300A and D-1400A, Shipley Company, Newton, Mass. 02162

19. Private Communication with S. Price of the Shipley Company, 27 April 1983.

20. G. J. Dunning and M. L. Minden, Appl. Opt. 19, 2419 (1980).

21. D. Gabor, Nature 161, 777 (1948).

22. J. W. Goodman, Introduction to Fourier Optics, McGraw-Hill Book Company, St. Louis, MI (1968).

23. R. J. Collier, C. B. Burckhardt, and L. H. Lin, Optical Holography, Academic Press, New York (1971).

24. R. Alferness, Ph.D. Thesis, University of Michigan, (1976), Xerox University Microfilms.

25. J. C. Urbach and R. W. Meier, Appl. Opt. 8, 2269 (1969).

26. H. Kogelnik, Bell Syst. Tech. J. 48, 2909 (1969).

27. M. G. Moharam, T. K. Gaylord, and R. Magnuson, J. Opt. Soc. Am. 70, 300 (1980).

28. B. J. Chang, Opt. Eng. 19, 642 (1980).

29. H. Nassenstein, Optik 30, 201 (1969).

30. W. Lee and W. Streifer, J. Opt. Soc. Am. 68, 795 (1978).

31. C. W. Chen and W. Sweatt, SPIE LASL Optics Conference 190, 5 (1979).

32. C. W. Chen, Opt. Eng. 19, 649 (1980).

33. I. Weingartner and K. J. Rosenbruch, SPIE Adv. in Opt. Production Technology 163, 73 (1979).

34. S. D. Fantone, Appl. Opt. 22, 1121 (1983).

35. A. Yi-Yan, J. A. Wilkinson, and C. D. Wilkinson, IEE Proc. 127, Pt. H. 335 (1980).

36. L. A. Jenkins, R. R. August, and D. B. Anderson, "Holographically Prepared Gratings For Integrated Optics", Rockwell International Corp. 55 (1974).

37. L. F. Johnson, Appl. Opt. 18, 2559 (1979).

38. P. D. DeGraff and D. C. Flanders, J. Vac. Sci. Technol. 16, 1906 (1979).

39. D. Heflinger, J. Kirk, R. Cordero, and G. Evans, Opt. Eng. 21, 537 (1982).

40. M. Wlodarczyk, Opt. Comm. 31, 125 (1979).

41. N. N. Efremow, N. P. Economou, K. Bezjian, S. S. Dana, and H. I. Smith, J. Vac. Sci. Technol. 19, 1234 (1981).

42. S. Matsui, K. Moriwaki, H. Aritome, S. Namba, S. Shin, and S. Suga, Appl. Opt. 21, 2787 (1982).

43. J. J. Hanak and J. P. Russell, RCA Review 32, 319 (1971).

44. Private Communication with B. Crane of the United States Air Force Academy, 12 May 1983 (by phone and letter of same date).

45. Private Communication with J. Schultz of the 3M Company, 23 August 1982.

46. K. Rabinovitch and A. Pagis, Appl. Opt. 21, 2160 (1982).

47. B. A. Moys, Thin Solid Films 21, 145 (1974).

48. B. E. Yoldas, Appl. Opt. 19, 1425 (1980).

49. C. J. Laan and H. J. Frankena, Appl. Opt. 21, 2809 (1982).

50. I. J. Hodgkinson and R. G. Stuart, Thin Solid Films 87, 151 (1982).

51. J. A. Dobrowolski and S. H. C. Piotrowski, Appl. Opt. 21, 1502 (1982).

52. Private Communication with B. Crane of the United States Air Force Academy, March 1983.

53. Handbook of Chemistry and Physics, Chemical Rubber Publishing Company, Cleveland, OH (1948).

54. Private Communication with D. Chen of Optical Peripherals, Colorado Springs, CO, March 1983.

55. R. Kastner and R. Mittra, IEEE Transactions on Antennas and Propagation AP-30, 673 (1982).

56. J. Hanfling, G. Jerinic, and L. Lewis, IEEE Transactions on Antennas and Propagation, AP-29, 622 (1981).

57. K. L. Tai, W. R. Sinclair, R. G. Vadimsky, J. M. Moran, and M. J. Rand, J. Vac. Sci. Technol. 16, 1977 (1979).

58. J. M. Moran and D. Maydan, J. Vac. Sci. Technol. 16, 1620 (1979).

59. Business Week, 40B (22 November 1982).

60. Lasers & Applications, 28 (November 1982).

61. Private Communication with S. Gilbert of University of Minnesota Microelectronics Laboratory, 12 May 1983.

62. G. R. Brewer, Electron Beam Technology in Microelectronics Fabrication, Academic Press, New York (1980).

63. S. K. Case, Ph.D. Thesis, University of Michigan, (1976), Xerox University Microfilms #76-27,461.

APPENDIX A

Holographic Integrated Circuit Masks

Conventional integrated circuit (IC) technology employs photographic techniques to transfer complex circuit patterns from a mask to silicon chips. The mask is much like a photographic negative. Current equipment uses expensive lenses (a hand-fitted lens for the latest stepping aligner costs $50,000[59]) which image the mask, often with reduction, onto a chip which has been coated with photoresist. Typically, ultraviolet (UV) light sources are used.

During the past few years, amazing progress has been made in packing more and more circuitry onto a given chip area. However, imaging systems are approaching diffraction limits and until recently it appeared that the semiconductor industry had thus reached a fundamental physical limit.

Using production techniques today, the most densely packed circuit elements contain lines spaced about 1.5 μm apart[60]. Using laboratory optical systems, line widths of 0.6 μm have been made[61]. However, by 1985 the demand for still smaller circuit elements is expected to create a need for lines as thin as 0.5 μm[60]; that is, smaller than the diffraction limit of current imaging technology.

A conventional lens has a diffraction limited focal spot of radius

$$r_f \cong 1.22\left(\frac{\lambda_o f_\ell}{w}\right) \tag{31}$$

where f_ℓ is the focal length of the lens and w is the lens diameter. Since the diffraction limit of an optical system can be reduced by using shorter wavelength light, one solution currently being studied is the use of excimer lasers which emit high power in the deep UV. IBM's San Jose Research Laboratory has already demonstrated that a Xenon-chloride laser can make submicron features with quality comparable to current UV photolithography. IBM's system has a limit of 0.3 μm. However, excimer lasers are big, bulky, and use dangerous gases such as fluorine[60].

Another way of reducing wavelength is by using X-rays. To date, line widths of 0.1 μm have been recorded in laboratory environments with X-rays[62]. However, X-ray sources are expensive and inefficient. In addition, formidable problems have been encountered in making X-ray masks which are stable and free of defects[60].

A third approach is electron beam lithography. Here an electron beam is used to expose resist-coated substrates. Line widths of 0.2 μm have been achieved under laboratory conditions[62] but the process is very slow since each line is drawn separately, as an overlapping series of dots[59].

We believe another solution is possible using visible light sources which are inexpensive compared to those used in the alternative proposals described above. Our proposal

is a parallel process in which the entire pattern is recorded simultaneously in resist using technology adapted from holography.

In this dissertation we report on optical elements which have 0.15 μm lines separated by 0.15 μm spaces. These are optical elements we now make routinely. The difference between our work and conventional photolithography is that our technique is a holographic rather than an imaging process. In holography the resolution limit is a spatial period of $\lambda_o/2$, as given by Eq. 16. Thus, using 457.9 nm light in air, 0.12 μm lines separated by 0.12 μm spaces are theoretically possible.

Development of a holographic based system to make ICs is a major project beyond the scope of our research. However, we wish to point the way to such research by demonstrating that holographic techniques can be successfully applied to circuit fabrication. Thus, in this appendix we report on the first step: the results of our efforts to produce a holographic circuit mask.

There are several advantages of holographic IC masks over conventional contact printing or step-and-repeat imaging IC systems. First, a holographic image is reconstructed in space, making it superior to contact printing. This aerial image can also be large in spatial extent, eliminating the need for step-and-repeat processing. Thus, the hologram combines the advantages of large size (an advantage

of contact printing) and the lack of physical contact between mask and wafer (an advantage of imaging systems). Secondly, because the hologram is recorded in a Fresnel plane, if a portion of a hologram is scratched or covered with dust or fingerprints, the scratch, dust or fingerprints do not appear in focus in the reconstructed image. At worst, the image resolution is slightly degraded over a small area. Thirdly, holographic reconstruction does not require the use of imaging lenses.

The idea of using holography to make ICs is not unique to us. Recently, we discovered that Insystems Inc. of San Jose, California has also started work on a holographic system to print ICs. However, Insystems is not openly discussing their technique, claiming that their system will not be available commercially for at least four to five years[59].

We believe the first step required to demonstrate the feasibility of holographic IC production is to show that a holographic mask can be made. Thus, that was our goal. Eventually, maskless holographic techniques, much like those used in this research to make diffraction gratings, may be possible.

To achieve our goal of making a holographic mask, we use, as our object, a conventional IC mask (a photographic negative of the IC on a glass substrate) and the experimental configuration shown in Fig. 41. A laser beam is coherently split into two beams by a beam splitter (BS). After

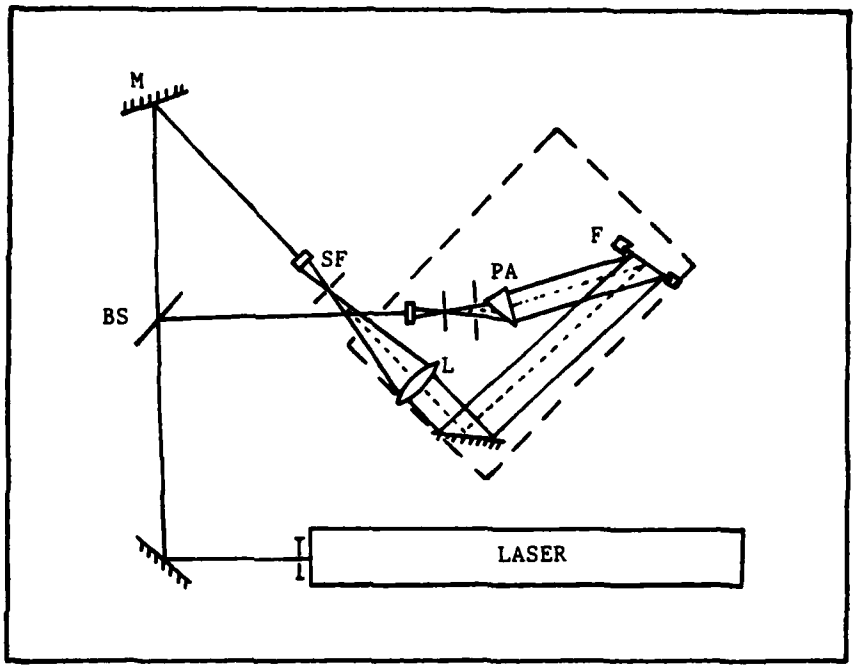

Fig. 41. Experimental Setup Used to Make Holographic IC Mask
Dashed Box in Drawing Corresponds to Photo

reflecting from carefully placed steering mirrors (M), each beam is then spatially filtered using a microscope objective and pinhole assembly (SF). An f/4 lens (L) is used to collimate one of the beams, known in holography as the reference beam. The object is placed in the other beam between the film holder (F) and the pinhole. To prevent undesirable interference, the film holder is oriented so that surface reflections from the film are not directed back into either beam. For similar reasons, the object is index matched to a prism which has an absorptive backing plate on one of its other faces. The prism assembly (PA) acts to displace undesirable surface reflections.

Exposures were made in dichromated gelatin. Dichromated gelatin has greater sensitivity and linearity than photoresist. Surface relief features, the major advantage of photoresist, are not needed in this application. Processing was as described in reference[63].

Following exposure and development, the object beam was blocked and the hologram was rotated 180° and placed in the film holder so that the reference beam illuminated the back of the holographic plate. This positioning is standard for holographic reconstruction of a real image[22]. A Kodak 649F film plate was placed in the plane of the reconstructed holographic image and exposed just as silicon wafers are exposed in conventional IC production. The Kodak plate was then developed in D-19 for 7 minutes, washed in water for

10 seconds, fixed in Kodak Rapid Fix for 5 minutes, washed in water for 10 minutes, and then rinsed in methanol for 2 minutes. Figure 42 is a picture of the original IC mask and Fig. 43 is a picture of the holographic copy recorded on the Kodak 649F plate. Since a holographic reconstruction is a positive rather than a negative image of the original object, the Kodak plate is essentially a negative of the original IC mask.

Note that the holographic copy contains all of the detail of the original mask and nearly the same resolution. These results demonstrate that holographic IC masks can be produced using standard holographic technology already available.

Our holographic mask has all of the advantages of holographic IC masks stated above although the redundancy of holograms, which accounts for the good performance of holograms even when dusty or scratched, is only minimally present in our hologram. Redundancy requires a diffuse object. Our object, a conventional IC mask, is not very diffuse. We have tried several techniques, such as illuminating the object with several divergent beams, designed to increase the effective diffusivity of the object. However, we have had only moderate success because following development, we cannot position the hologram in our holder with enough precision. A more expensive holder will be necessary to continue this approach.

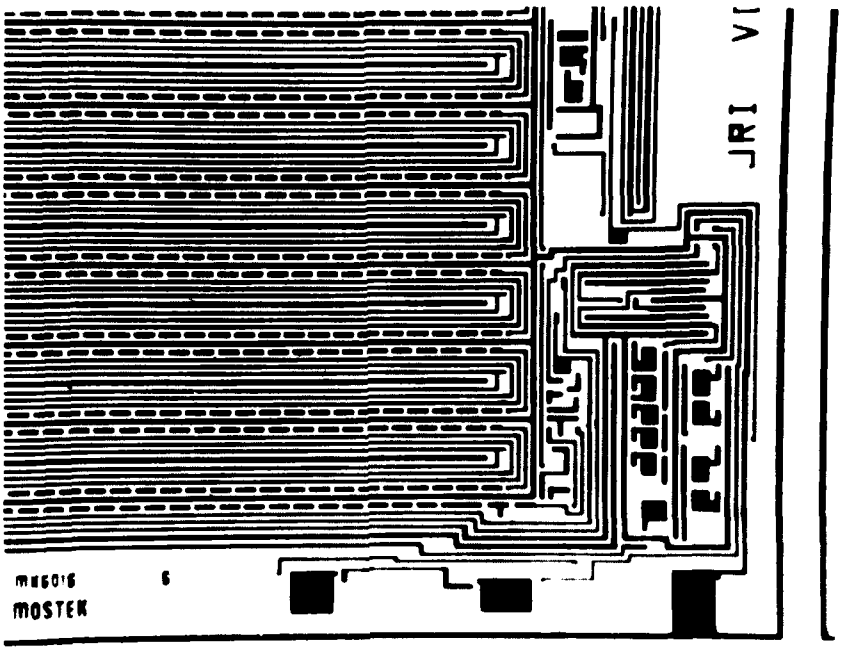

Fig. 42. Original IC Mask

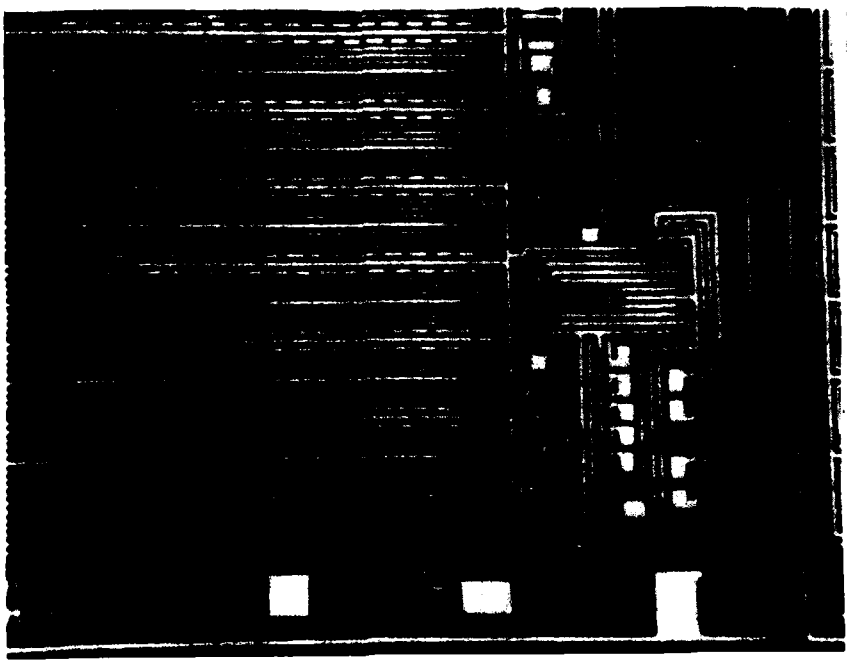

Fig. 43. Pattern Produced from Holographic IC Mask. Pattern was Recorded on Kodak 649F Film

Our research demonstrates the potential of holography to the microelectronics industry. Now that we have proven holographic IC masks can be made, the next step is to demonstrate that masks with smaller features sizes can be holographically recorded. However, the real advantage of holography will come when no mask is made but instead, fine lines, similar to those recorded for our photoresist gratings, are recorded directly onto photoresist coated wafers. Such a process will require a large number of coherent beams, each of precise irradiance and phase. It is likely to be a difficult problem, but when completed will be theoretically capable of producing 0.12 μm line widths with visible light in air.

Vita

Rolf Enger was born on 14 November 1949 in Sheboygan, Wisconsin, the son of Carl and Henrietta Enger. He graduated from Sheboygan North High School, Sheboygan, Wisconsin in 1968. Upon completion of the necessary course work in 1972, he received the degree of Bachelor of Arts, Summa Cum Laude, in Physics, from St. Olaf College. Also upon graduation, he received a commission in the United States Air Force through the ROTC program. In July 1972 he was assigned to the 44th Strategic Missile Wing at Ellsworth Air Force Base, South Dakota. While at Ellsworth, he served as a missile combat crew commander, as a deputy missile combat crew commander, and as a missile combat crew instructor. As a missile officer, he was in direct command and control of up to 50 Minuteman Intercontinental Ballistic Missiles. In May 1976 he married Lois Renée Wolf and on 18 September 1977 the couple was blessed by the birth of their first daughter, Tiffany Faye. In December 1977 Rolf was awarded the degree of Master of Science in Engineering Physics from the Air Force Institute of Technology as a Distinguished Graduate. In January 1978 he joined the faculty at the United States Air Force Academy, where he served as an Instructor and Assistant Professor of Physics until coming to the University of Minnesota in September 1980. During the course of his study at the University, Rolf and Lois were again blessed with a daughter, Holly Renée, on 18 July 1982.

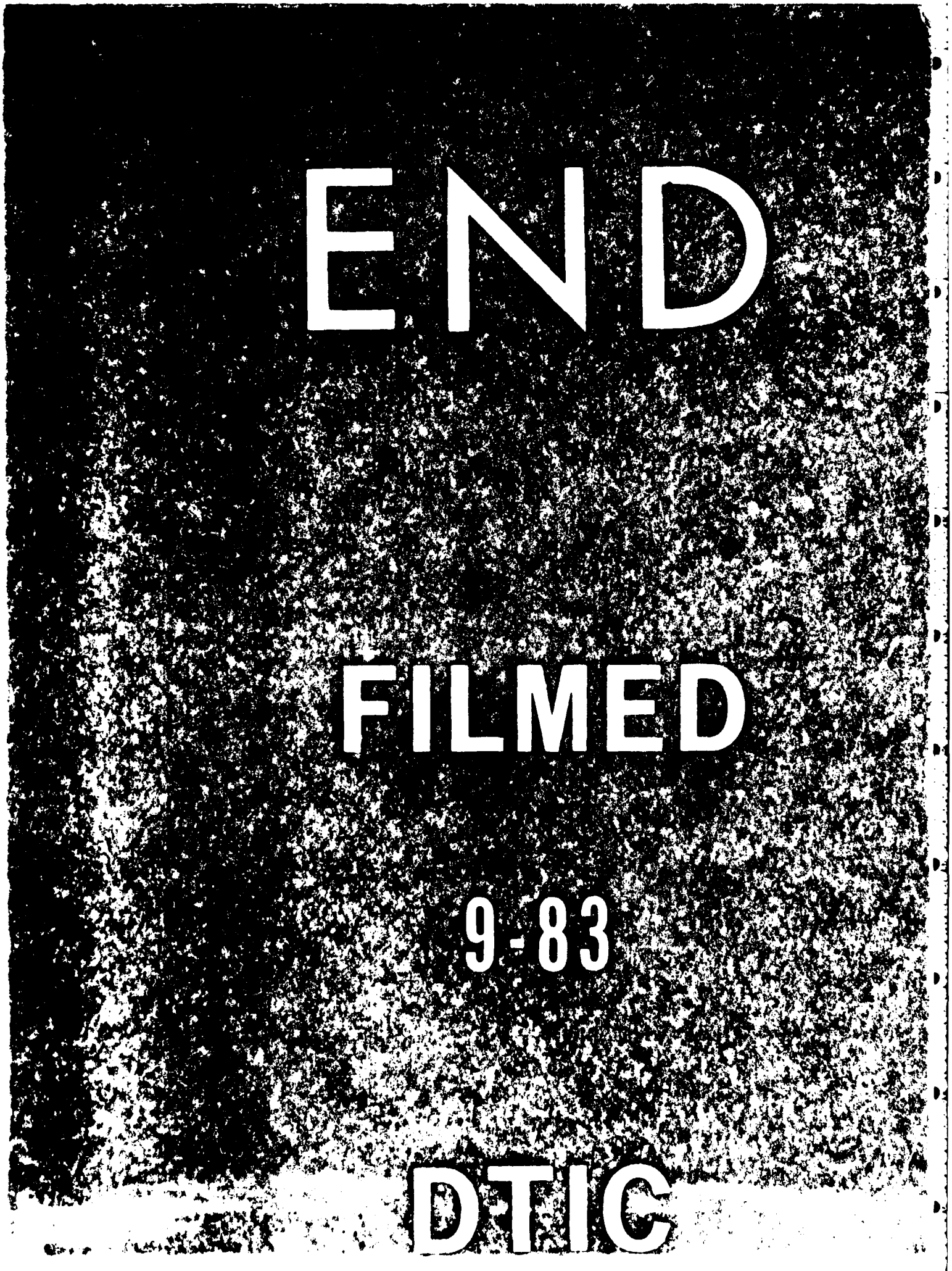
END
FILMED
9-83
DTIC